Catalysis Science & Technology

www.rsc.org/catalysis

Volume 2 | Number 9 | September 2012 | Pages 1721–1996

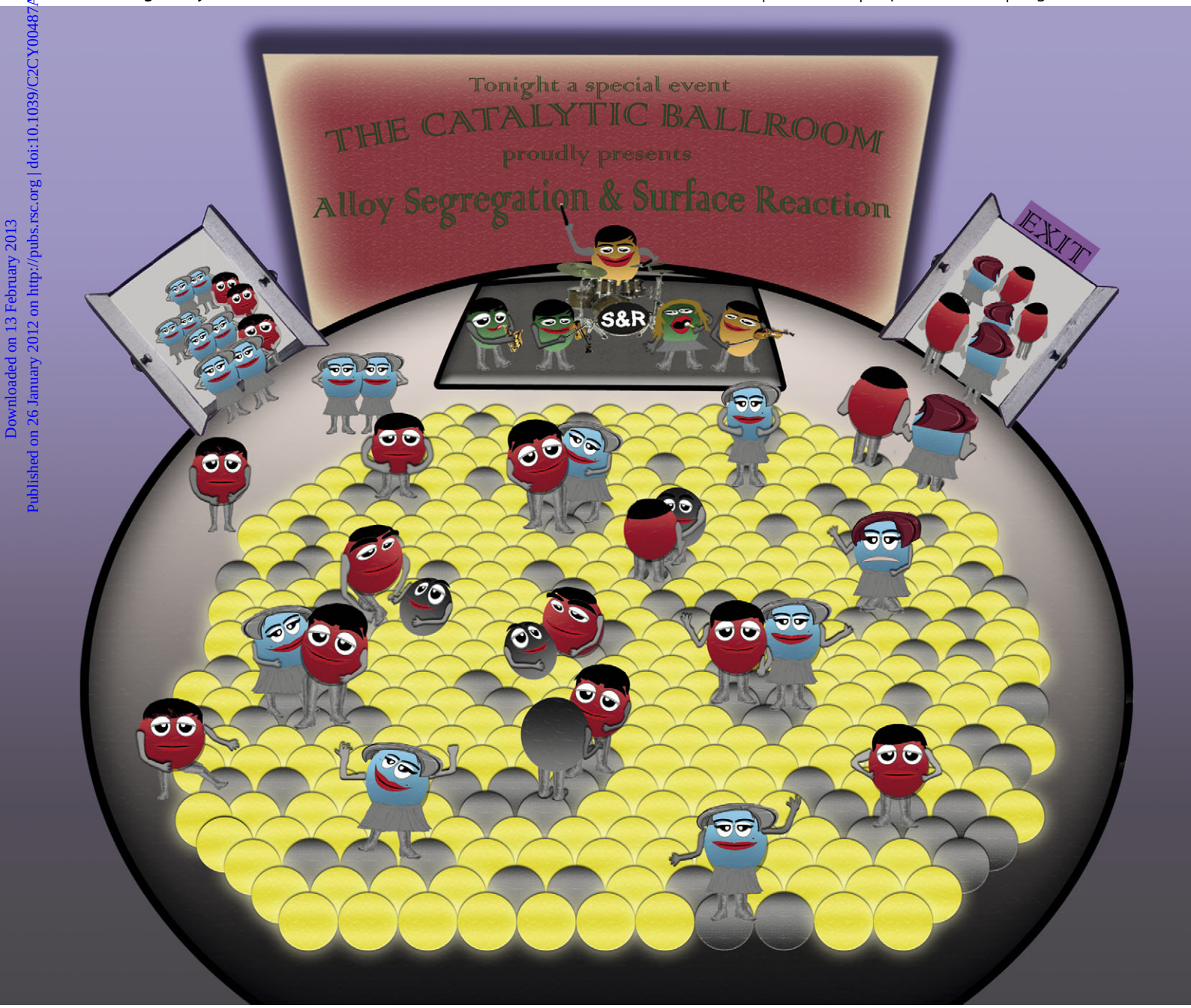

ISSN 2044-4753

COVER ARTICLE
Zafeiratos, Piccinin and Teschner
Alloys in catalysis: phase separation and surface segregation phenomena in response to the reactive environment

RSC Publishing

2044-4753(2012)2:9;1-6

Catalysis
Science & Technology

Cite this: *Catal. Sci. Technol.*, 2012, **2**, 1787–1801

www.rsc.org/catalysis

MINIREVIEW

Alloys in catalysis: phase separation and surface segregation phenomena in response to the reactive environment

Spiros Zafeiratos,*[a] Simone Piccinin[b] and Detre Teschner*[c]

Received 25th November 2011, Accepted 23rd January 2012
DOI: 10.1039/c2cy00487a

Alloys play a crucial role in several heterogeneous catalytic processes, and their applications are expected to rise rapidly. This is essentially related to the vast number of configurations and type of surface sites that multi-component materials can afford. It is well established that the chemical composition at the surface of an alloy usually differs from that in the bulk. This phenomenon, referred to as surface segregation, is largely controlled by the surface free energy. However, surface energy alone cannot safely predict the active surface state of a solid catalyst, since the contribution of other parameters such as size and support effects, as well as influence of the adsorbates, play a major role. This can lead to numerous surface configurations as for example over the length of a catalytic reactor, as the chemical potential of the gas phase changes continuously over the catalyst bed and hence different reactions may prevail at different catalyst bed segments. Thanks to the rapid improvement of the analytical surface science characterization techniques and theoretical methodologies, the potential effects induced by alloyed catalysts are better understood. For catalysis, the relevance of measurements performed on well-defined surfaces under idealized ultrahigh vacuum conditions has been questioned and studies in environments that closely resemble conditions of working alloy catalysts are needed. In this review we focus on experimental and theoretical studies related to *in situ* (operando) observations of surface segregation and phase separation phenomena taking place on the outermost surface layers of alloy catalysts. The combination of first principles theoretical treatment and *in situ* observation opens up new perspectives of designing alloy catalysts with tailored properties.

1. Introduction

Development of new materials with improved performance is one of the main objectives of research in catalysis. In heterogeneous catalysis, catalysts containing two or more metals might show significantly different catalytic properties compared to the parent metals and thus are widely utilized in several reactions including reforming,[1] pollution control[2] and alcohol oxidation.[3] One of the most attractive aspects of using multi-metallic catalysts is the possibility of rationally designing the catalytic properties by controlling the type and composition of the elements.[4,5] A detailed knowledge of the catalyst surface is a crucial first step in this approach and therefore has been the focus of numerous studies as summarized in several earlier reviews.[6–13] Since the definition of different types of multimetallic materials is not very consistent in the literature, throughout this manuscript an "intermetallic compound" refers to a chemical compound of two or more metallic elements which adopts (at least partly) an ordered crystal structure that differs from those of the constituent metals. On the other hand, an "alloy" is a mixture of metals, intermetallic compounds and/or non-metals, and thus it can contain more than one phase. The term "bimetallic" refers to an alloy of two metals.

Two main models have been put forward in order to explain the modification of the chemical properties of a metal in a bimetallic surface. First, the formation of the hetero-atom bonds changes the electronic environment of the metal surface, through the *electronic* (*or ligand*) *effect*. A second explanation is the so-called *geometric* (*or ensemble*) effect. According to this model, incorporation of atoms with different reactivity patterns on a bimetallic surface not only gives rise to strain effects, but also decreases the number of available multiple absorption sites (3-fold, 2-fold, in favour of single atom sites), modifying the chemisorption and reaction properties of adsorbates (ref. 14 and references therein). In general, differentiation between ensemble and electronic effects is rarely clear and often there is a contribution from both effects.

Although bulk alloys have been thoroughly studied and phase diagrams predicting the thermodynamic conditions for

[a] *Laboratoire LMSPC, UMR7515 CNRS-Université de Strasbourg, 25 rue Becquerel, 67087 Strasbourg, France. E-mail: spiros.zafeiratos@unistra.fr; Fax: +33 39024 2761; Tel: +33 36885 2755*
[b] *CNR-IOM, Istituto Officina dei Materiali, Via Bonomea 265, 34136 Trieste, Italy*
[c] *Fritz-Haber Institute of the Max Planck Society, Department of Inorganic Chemistry, Faradayweg 4–6, Berlin, D-14195, Germany. E-mail: teschner@fhi-berlin.mpg.de; Fax: +49 30 8413 4676; Tel: +49 30 8413 5408*

alloy formation in the bulk are well established, the composition of a bimetallic surface may be significantly different compared to the bulk material. This phenomenon is usually described as surface segregation (or just segregation). These differences are being driven by a complex interplay of both *thermodynamic parameters*, such as the relative surface energies, the bonding strengths of each metallic component with adsorbed atoms and molecules, the tendency of the metal components to form ordered alloy phases, and *kinetic parameters* such as diffusion barriers. Therefore, stable bulk alloys may exhibit phase separation on their surfaces and *vice versa*. For example, metals that are almost immiscible in the bulk, such as Au and Ni, showed evidence of extended bimetallic interaction on the surface (surface alloy).[15] As a simple rule of thumb the element with the lowest surface energy segregates to the surface under vacuum conditions.

Alloy catalysts, however, typically operate under high pressure and high temperature conditions, and these reactive environments may substantially influence the alloy surface composition. If reactants interact strongly with one of the alloy constituents, the surface tends to be enriched in that constituent, even when it is not predominant in an inert atmosphere (adsorbate-induced surface segregation). Moreover, small excesses of one element with respect to the others in the bulk alloy compared to the nominal composition, or other bulk defects, can also play a role, especially in strongly ordered compounds.[16] The combined effects of the gas-phase atmosphere and the bulk alloy properties will therefore determine the composition and oxidation state of the alloy surface. An example of the modification induced by high pressure conditions is the development of an oxide like film at the catalyst surface of several transition metals (*e.g.* Ru, Pd, Ag) encountered in oxidation catalysis.[17–19] Reaching the active state of the catalyst may require a considerable induction period, which reflects the large modifications resulting from the interaction of the metal surface with the reaction environment.

In the following review we summarize recent experimental and theoretical work focusing on the description of bimetallic and ternary, extended and nanosized, alloy surfaces under reactive gas phase environments. Emphasis will be given to studies performed at catalytically relevant conditions (elevated temperature and pressure) using *in situ* applied surface sensitive techniques.

2. Methods

2.1. Experimental approaches

Traditionally, *in situ* studies of solids under realistic liquid or gas phase environments were performed by using experimental techniques based on photons, like for example UV-Vis, Extended X-ray Absorption Fine Structure (XAFS) and Raman spectroscopies, *etc.* The use of photons as a probe was implied by the fact that they do not interact strongly with matter (of course this is also related to their energy) and therefore in a large extent could go through the gas or liquid environment above the sample. These techniques are however not particularly sensitive to the surface and probe a large volume of the solid. Techniques based on low and medium energy electron probing are better suited for surface sensitive studies, but until recently most of them were confined in vacuum environments. In the last few years, several microscopic and spectroscopic techniques capable to operate *in situ* and deliver atomic-scale information on solid surfaces or nanoscale materials were developed and a recent review about their impact on our understanding of surface chemistry is given by Tao and Salmeron.[20] Below we briefly describe aspects of selected *in situ* techniques cited in this article to facilitate the comprehension.

2.1.1. Ambient pressure X-ray photoelectron spectroscopy (APPES). As opposed to classical Photoelectron Spectroscopy (PES) requiring ultra-high vacuum (UHV) conditions, using differential pumping in APPES the surfaces can be investigated in the presence of gases and vapours at a pressure of currently up to ~10 mbar.[21,22] This maximum pressure is a strong function of experimental and technical parameters like type of gas, quality of surface, available photon flux, diameter of the first aperture (and thus the distance to the sample), acceptance angle of the electron analyzer, type of detector, *etc.* Usually, samples at any relevant temperature (RT—1000 K) can be studied. Recently, most experiments are performed at synchrotron sources, which allows varying the excitation energy and thus by recording different kinetic energy electrons the information depth can be modulated.

2.1.2. X-Ray absorption near edge structure (XANES). Absorption experiments in the soft X-ray energy range when performed using (Auger, partial or total) electron yield collection can be nearly as surface sensitive as the corresponding PES probing. A very recent demonstration suggests that such experiments can indeed be carried out at pressures up to 1 bar.[23] Since absorption probes the local electronic structure at the excited state, even small differences can be recognized; nevertheless interpretation may be challenging and may require theoretical simulations. In contrast to APPES, XANES in the soft X-ray regime cannot be applied for all elements (due to the lack of sensitive transition), and it is more difficult to quantify the results.

2.1.3. Fourier transform infrared spectroscopy. FT-IR, with its various forms (DRIFTS, PM-IRAS, *etc.*), has been widely applied to investigate surfaces under relevant operation conditions. Its advantage, due to the long photon mean free path, is the easy adaptation to the required experimental conditions, however the limitation is that information is indirect in the sense that not the material itself but rather the surface functional groups are analyzed.

2.1.4. High-pressure scanning tunneling microscopy. STM based on quantum tunneling allows for imaging flat surfaces at atomic resolution. STM cells can be operated at atmospheric pressure and realistic temperature; nevertheless resolution is compromised at elevated temperature and pressure.

2.2. Theoretical approaches

The structure and composition of bimetallic surfaces in vacuum was the focus of early first-principles calculations, based on density functional theory (DFT) using the coherent-potential approximation and on effective-medium theory[24] as well as on the Green's-function linear-muffin-tin-orbital (LMTO) approach.[25] In these studies the authors computed the derivatives of the surface

energy *versus* surface concentration: the first derivative is the surface segregation energy (which determines whether an impurity segregates to the surface or not) and the second derivative is the surface mixing energy (which determines whether the two elements mix at the surface or phase-separate, forming islands). These results were used to construct a complete database of the segregation energies and the surface mixing energies for all combinations of the transition metals, which have been instrumental in rationalizing the surface composition of different bimetallic alloys in experiments as well as in designing new materials.[4,5] The role of the reactive environment in the structure and composition of the alloy surfaces, however, was not investigated in these earlier studies.

In this section we will briefly review two well established methodologies, both based on a DFT description of the electronic structure of the system, that have been employed to theoretically model the equilibrium structure of metal surfaces, and alloys in particular, in a reactive environment.

In the first approach, called *ab initio* atomistic thermodynamics, one considers a portion of the system (the surface) to be in contact with a gas phase atmosphere and with a bulk phase, and computes the surface free energy of several candidate surface structures to determine the most stable under specific conditions of temperature, partial pressures of the gas phase species and chemical potentials of the bulk phase elements.

A second approach is the lattice-gas-Hamiltonian (also called cluster expansion) method, where a polynomial expansion of the energy of the system is parametrized in terms of a set of DFT calculations. This enables us to study many more and much larger surface structures compared to the previous approach, properly accounting for disorder and configurational entropy effects, but is limited to the treatment of structures with a pre-determined lattice topology.

2.2.1. First-principles atomistic thermodynamics. The basic features of this approach will be illustrated for the case of a bi-component alloy, AB, in thermodynamic equilibrium with an oxygen gas atmosphere. The generalization to multicomponent alloys is obvious, while for the case of a gas phase containing multiple species we refer the reader to the recent literature.[26,27] The surface, a portion of the whole system containing $N = N_A + N_B$ atoms at x_A and x_B molar fractions, is considered to be in thermodynamic equilibrium with both the gas atmosphere (held at temperature T and pressure p) and the underlying bulk alloy. The most stable surface structure is the one that minimizes the surface free energy $\gamma(T,p)$, defined as

$$\gamma(T,p) = 1/A_{surf}[G(T,p,N_A,N_B,N_O) - N_A\mu_A - N_B\mu_B - N_O\mu_O(T,p)] \quad (1)$$

Here, G is the free energy of the portion of the system being considered, μ_A, μ_B and μ_O are the chemical potentials of A, B and O atoms, respectively, and the surface free energy is normalized by the surface area A_{surf}. The chemical potential of the oxygen atoms is determined by the gas phase reservoir, $\mu_O = 1/2\mu_{O_2(gas)}(T,p)$, which can be described to a sufficient degree of approximation as an ideal gas:

$$\mu_{O_2(gas)}(T,p) = E^{total}_{O_2(gas)} + 2\Delta\mu_O(T,p^0) + k_B T \ln(p/p^0) \quad (2)$$

where k_B is the Boltzmann constant, p^0 is the standard pressure (1 atm) and the term $\Delta\mu_O$ can be obtained from the experimental temperature dependence of the enthalpy and entropy.[28] The oxygen chemical potential in the gas phase, $\mu_{O_2(gas)}$, controls the effect of the gas atmosphere on the structure and composition of the surface. O-rich environments, corresponding to higher values of $\mu_{O_2(gas)}$, will favour structures containing a higher number of oxygen atoms per unit area. Under O-poor conditions, corresponding to sufficiently low values of $\mu_{O_2(gas)}$, clean surfaces without oxygen atoms will become stable.

The free energy comprises several terms that need to be evaluated separately:

$$G = E^{total} + F^{vib} - TS^{conf} + pV \quad (3)$$

where E^{total} is the total energy, F^{vib} is the vibrational contribution to the free energy, S^{conf} is the configurational entropy (*i.e.* the entropy due to the number of different configurations in which the constituents can be arranged in the given lattice). The last two terms are typically neglected,[29] and the vibrational contributions are usually below 10 meV Å^{-2} in the 0–1000 K temperature range[29,30] and therefore also neglected. The free energy term G is therefore usually approximated by the total energy E^{total}, and temperature and pressure effects enter only through the chemical potential of the oxygen reservoir, through eqn (2).

The total energy, E^{total}, is normally evaluated using quantum-mechanical DFT calculations, which offer the best compromise between the accuracy required to simulate processes like the adsorption/desorption of the gas phase species and computational feasibility. Moreover, one is typically interested in computing the relative stability of different surface structures (*i.e.* surface energy differences) rather than absolute values of surface energies, so some degree of error cancellation can be expected. Absolute values, on the other hand, are more sensitive to the intrinsic errors due to the approximations in the exchange and correlation (XC) functional employed in DFT. It also worth mentioning that computing the value of the chemical potential of the oxygen reservoir is problematic in calculations that employ generalized gradient approximation (GGA) functionals such as PBE.[31] The binding energy of the oxygen molecule is in this case overestimated by about 0.5 eV per O atom, which translates into a severe error bar in the determination of temperatures and pressures in the phase diagrams. This error, however, will be partially compensated by the analogous GGA error in the description of oxygen chemisorbed on the metal surfaces.

In these calculations the system is described using a slab geometry in small unit cells periodically repeated in space; therefore only ordered structures can be simulated in this approach. Furthermore, when dealing with surface alloys or overlayers formed by impurity atoms introduced at the surface of the hosting metal, such small unit cells cannot accommodate large deformations that might be induced by, for example, size mismatch between the host and the impurity atoms, thus leading to large stresses in the overlayers.

2.2.2. Lattice-gas-Hamiltonian. In cases where disordered structures need to be considered, chemical equilibrium requires sampling a large configurational space, which prevents a fully first principles treatment to be applicable. Fortunately, a well

established technique exists to parametrize the energy of a system that can be mapped in a regular lattice. This approach, named "cluster expansion" or "lattice gas Hamiltonian",[32] involves the use of a set of DFT calculations of a few ordered arrangements of atoms on an underlying fixed topology to extract the many-body interaction terms that enter the Hamiltonian of the system. For example, in the case of a binary alloy A–B, we can define the occupation variables n_i to have the value 1 or −1 depending on whether site i is occupied by atom A or B. A cluster expansion of the Hamiltonian of the system consists in an expansion of the energy of the system in terms of polynomials of the variables n_i:

$$H^{\mathrm{LGH}} = V^1 \sum_i n_i + \sum_{m=1}^{r} V_m^2 \sum_{\langle ij \rangle_m} n_i n_j + \sum_{m=1}^{q} V_m^3 \sum_{\langle ijk \rangle_m} n_i n_j n_k \qquad (4)$$

The V^1, V_m^2, V_m^3, *etc*. terms represent the many-body terms involving one, two, three, *etc*. terms, respectively. The m index indicates that for each of these terms one needs to consider several types of interactions. For example, in the case of two-body terms, V_m^2, one needs to consider nearest-neighbours interactions, second nearest-neighbours interactions and so on. These polynomials can be shown to form a complete basis, making this expansion formally exact. While in principle the cluster expansion includes an infinite number of terms and summations, in practice it can be truncated, since higher order and longer distance interactions are typically found to be negligible compared to lower order and shorter distance interactions. To select which terms to include in the cluster expansion and to evaluate its accuracy, validation schemes such as the leave-one-out cross validation (LOO-CV) approach are used.

Once the lattice-gas-Hamiltonian has been constructed, it can be used to study large ordered or disordered systems at finite temperatures with Monte Carlo simulations, either in the canonical[33,34] or gran-canonical[35] ensembles. In the latter case, in particular, the surface segregation properties of an alloy can be studied as a function of the environment, as we will see in Section 3.1.3.

3. Examples

3.1. Selected theoretical studies of bi-metallic alloys in an oxygen atmosphere

In the following we will review three systems that have been investigated using the theoretical methodologies described above: the Ag–Cu and the Ag_3Pd alloys in an oxygen atmosphere, studied using the *ab initio* thermodynamics method and the Pt–Ru alloy again in an oxygen atmosphere, studied using the lattice-gas-Hamiltonian method. The first example, in particular, will show how experimental and theoretical approaches can complement each other in a synergic effort to unravel the structure of an alloy in a reactive environment.

3.1.1. Ag–Cu alloys. In the production of ethylene oxide, an important chemical obtained through partial oxidation of ethylene, a key issue is to selectively promote the formation of desired product (ethylene oxide) while avoiding the formation of acetaldehyde, which is readily converted to carbon dioxide, the latter being the thermodynamically favoured pathway. In the chemical industry the catalyst of choice for this process is silver, which has a selectivity of around 40–50% when pure and of around 80% in the presence of alkali and chlorine promoters. Barteau and co-workers, however, found that alloying Ag with other metals, and in particular with Cu, can lead to a substantial increase of the selectivity toward the formation of ethylene oxide.[36,37]

Considering the (111) surfaces of Ag and Cu, due to the fact that the surface energy of silver is considerably lower than the one of copper (experimental values: $\gamma_{\mathrm{Ag(111)}} = 0.078$ eV Å^{-2} and $\gamma_{\mathrm{Cu(111)}} = 0.114$ eV Å^{-2}), the surface of the alloy is expected to expose Ag under UHV conditions. Indeed, the deposition of a Cu thin-film on Ag(111) in ultra high vacuum (UHV) leads to the formation of Cu islands encapsulated by one monolayer of Ag.[38,39]

On the other hand, experiments carried out on Ag–Cu alloys with 0.11% Cu content at ~500 K show that in an oxidizing environment the Cu surface content is in the 0.1–0.75 ML range,[36] much higher than expected from the bulk Cu concentration. The overall effect of the oxygen atmosphere is therefore to promote the segregation of Cu to the surface.

Using the *ab initio* atomistic thermodynamics approach, Piccinin *et al*. have studied the surface structure of the Ag–Cu alloy in the presence of oxygen.[40–42] They have shown that the strength of Cu–O bond relative to the Ag–O bond drives the segregation of Cu to the surface. Their main finding is that under conditions of pressure and temperature relevant for ethylene epoxidation, a thin copper-oxide-like layer is predicted to form at the surface. Several energetically similar structures

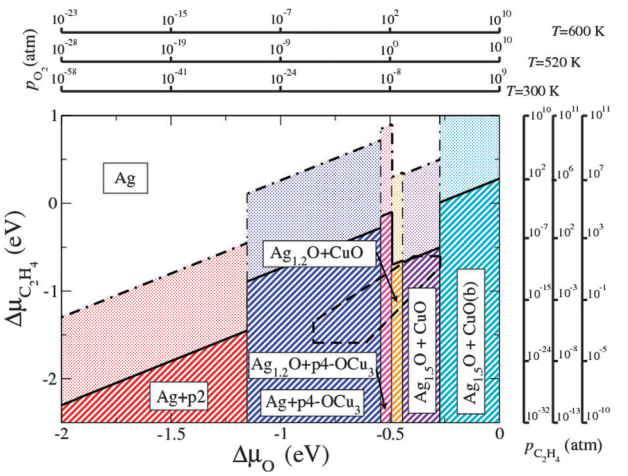

Fig. 1 Surface phase diagram for the (111) facet under constrained thermodynamic equilibrium with oxygen and ethylene. Solid (dot-dashed) lines represent the stability limit with respect to the formation of Ac (EO). Each shaded area represents the region of stability of a combination of two surface structures giving a Cu coverage of 0.5 ML. The white area is the region of stability of the clean Ag(111) surface. The dashed polygon corresponds to typical values of temperature and pressures used in experiments (T = 300–600 K and pO_2, $pC_2H_4 = 10^{-4}$–1 atm). $Ag_{1.2}O$ and $Ag_{1.5}O$ are 1-layer thin oxide-like structures; CuO and CuO(b) are 1-layer thin and bulk CuO structures, respectively; $p2$ and $p4$-OCu_3 are 1-layer thin Cu_2O-like structures with (2 × 2) and (4 × 4) periodicity, respectively. In the latter, an OCu_3 unit is removed. Reproduced with permission from ref. 42.

have been predicted, each of them bearing little resemblance with either bulk cuprous (Cu_2O) or cupric (CuO) oxide phases (see Fig. 1). APPES experiments on copper–silver nanopowder (~100 nm, 2.5 wt% Cu) at 520 K in O_2 as well as in $C_2H_4:O_2$ (1 : 2) atmospheres at a total pressure of 0.5 mbar confirmed the presence of a thin copper-oxide layer at the surface of the alloy.

An *ab initio* atomistic thermodynamics study of the Ag–Cu in the presence of both reactants in ethylene epoxidation has been carried out by Nguyen *et al.*,[27] showing that the thin surface oxide layer is thermodynamically stable also in the presence of ethylene, at the partial pressures and temperatures typically used in practical applications. The mechanism of epoxidation catalyzed by these and other surface structures has also been investigated theoretically using DFT calculations.[43–48]

3.1.2. Ag–Pd alloys. The *ab initio* atomistic thermodynamics approach has been used also by Kitchin *et al.*[49] to investigate the properties of the $Ag_3Pd(111)$ alloy surface in an oxygen atmosphere. The authors modelled the system using a (2 × 2) unit cell in which the composition of the first two surface layers was changed between pure Ag and pure Pd, and oxygen coverages in the O–1 ML range were considered. In this work the dependence of the surface structure and composition was studied as a function of both the chemical potential of the oxygen reservoir and the chemical potential difference between Pd and Ag. While the surface of the alloy is in thermodynamic equilibrium with the bulk Ag_3Pd alloy, small deviations from the nominal stoichiometry or the presence of local defects can modify the chemical potential of the elements in the bulk reservoir. Two extreme conditions were therefore considered, Pd-rich and Ag-rich conditions, defined by having values of one of the two elements equal to the corresponding pure bulk phase in an fcc structure ($\mu_{Pd} = \mu_{Pd,fcc}$ for Pd-rich conditions and $\mu_{Ag} = \mu_{Ag,fcc}$ for Ag-rich conditions).

Not surprisingly, under UHV conditions the more noble metal, Ag, is found to segregate to the surface. As the chemical potential of oxygen is increased, however, the adsorption of oxygen drives the segregation of Pd to the surface, increasing the Pd concentration in the first two layers. As in the case of the Ag–Cu alloy, there is a competition between the tendency of segregating the more noble metal to the surface and the tendency to lower the surface free energy by segregating the element that makes a stronger bond with the adsorbed oxygen.

The authors examined also the role played by the chemical potentials of the elements in the bulk alloy. As can be seen from Fig. 2, while under Pd-rich conditions (left panel) the onset of oxygen adsorption corresponds to the segregation of Pd to the surface, under Ag-rich conditions (right panel) oxygen adsorbs first on a Ag-pure surface and Pd segregation is induced only when a higher oxygen coverage is reached. The stabilization of Pd–O structures at the surface of the alloy takes place at a higher oxygen chemical potential compared to the Pd-rich case, reflecting the higher energetic cost to remove Pd atoms from an Ag-rich bulk phase. Moreover, the sequence of surface structures obtained by sweeping the values of oxygen chemical potential is different in the two cases, stressing how both the effects of the reactive environment and the bulk alloy structure need to be accounted for.

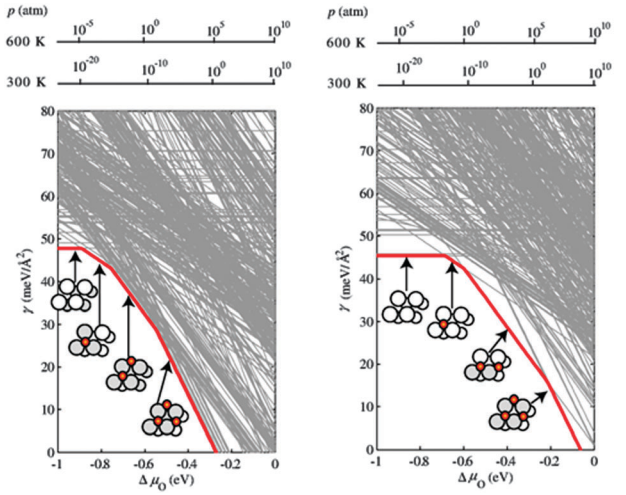

Fig. 2 Surface free energy of $Ag_3Pd(111)$ in equilibrium with a Pd-rich Ag_3Pd bulk reservoir, as a function of oxygen chemical potential. Each line corresponds to one of the tested surface configurations, and only the few configurations that result as most stable for a range of oxygen chemical potential are drawn as dark (red) lines. Additionally shown as insets are top views of the most stable surface configurations, with adsorbed O atoms shown as red small circles, Ag atoms as white circles, and Pd atoms as grey circles. The dependence on the oxygen chemical potential is translated into pressure scales for T = 300 K and T = 600 K (upper x axes). The left panel corresponds to Pd-rich Ag_3Pd bulk reservoir conditions, the right panel to Ag-rich conditions. Reproduced with permission from ref. 49.

One interesting point discussed by Kitchin *et al.* in their work is the fact that the onset of bulk oxidation of Pd in the Ag_3Pd alloy, resulting in PdO, is predicted to take place at values of oxygen chemical potential that are only slightly higher than those corresponding to oxygen adsorption of the surface of the alloy. This is quite different from what happens on pure Pd surfaces, where the adsorption of oxygen takes place at values of oxygen chemical potential well below the onset of oxidation. This is due to the higher cost to segregate Pd in Ag_3Pd, where Pd is scarce, compared to pure Pd. This therefore suggests that the segregation of Pd to the surface is likely to be accompanied by the formation of bulk-like oxide films at the surface.

One restriction of this approach is the fact that these types of studies are limited to a few periodic structures in a small unit cell, so that the configurational entropy contribution or intermediated coverages cannot be considered. These limitations can be circumvented by the use of the lattice-gas-Hamiltonian (or cluster expansion) method, as we will see in the next section.

3.1.3. Pt–Ru alloys. Ru–Pt alloys are important catalysts for the electro-oxidation of methanol in fuel cells. Moreover, Pt catalysts for CO oxidation are often alloyed with other transition metals such as Ru to enhance their tolerance to CO poisoning. In both cases the knowledge of the segregation profile and surface structure of the alloy in an oxygen atmosphere is crucial. Han *et al.* have investigated the properties of the Pt–Ru alloy surfaces in an oxygen atmosphere employing a first-principles-based lattice gas Hamiltonian in gran-canonical Monte Carlo simulations.[35] A set of 127 structures were used to obtain the cluster expansion, which contained 40 terms and

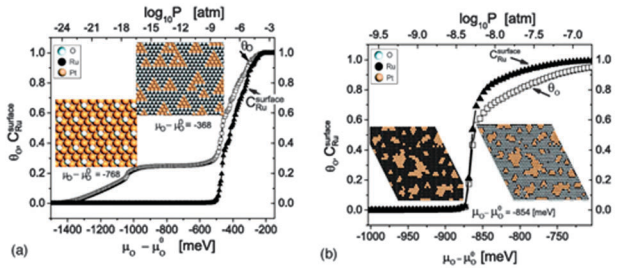

Fig. 3 Monte Carlo simulations and surface structure evolutions as a function of oxygen chemical potential μ_O, T and bulk Ru composition C_{Ru}. The conditions of (a) are T = 600 K, μ_{Ru} = 1750 meV and (b) T = 1050 K, μ_{Ru} = 665 meV. Reproduced with permission from ref. 35.

reproduced the DFT energies with a root-mean-square error of 8 meV and a CV of 15 meV. A Pt(111) surface in equilibrium with a Ru reservoir at chemical potential μ_{Ru} and an oxygen atmosphere at chemical potential μ_O was simulated using a large periodic cell as a function of μ_{Ru} and μ_O. While it is known that Pt has the lower surface energy and is therefore expected to segregate to the surface in vacuum, things drastically change in the presence of oxygen. The strong binding between Ru and O at the surface overcomes the higher surface energy of Ru compared to Pt, leading to an inversion of the segregation profile. By increasing the oxygen chemical potential, corresponding to increasing the oxygen pressure or lowering the temperature, Han *et al.* found that at low Ru chemical potentials the oxygen coverage increases, which gradually induces Ru to segregate to the surface.

At high values of Ru chemical potentials, on the other hand, the oxygen surface coverage and ruthenium surface composition are strongly coupled, both increasing abruptly above a critical value of oxygen chemical potential (see Fig. 3). One interesting finding is that while at low oxygen chemical potentials Ru segregates to the surface in the form of isolated atoms, at higher values the Ru atoms cluster together, resulting in islands of Pt surrounded by oxygen-covered Ru regions. This can be relevant for catalysis, since at the edges between Pt and Ru–O islands both Pt sites for the decomposition of methanol and oxygen for the oxidation reactions are available.

One important consideration stressed by Han *et al.* in their work is the assumption of thermodynamic equilibrium as well as sufficient mobility of Ru through the bulk necessary to allow the segregation to the surface. Industrial catalysts, on the other hand, might operate far from equilibrium, since they are prepared through a series of low-medium temperature steps to retain their small particle size and avoid sintering. Moreover, diffusion of oxygen adsorbates below the surface and the formation of surface oxides have been neglected, which could be important, especially at high values of oxygen chemical potentials.

3.2. Single feed experiments

The simplest approach to understand the effect of the catalytic reaction feed (usually a mixture of two or more gases) on the surface structure and composition is to describe the interaction of an alloy with a single gas atmosphere that thought to dominate gas–solid interaction. Typically, gases can be classified as oxidant (NO, O_2), reducing agent (CO, H_2) or inert (He, N_2), with UHV resembling reducing conditions. Below we will describe the relation between the composition, structure and chemical state at the surface of alloys upon their interaction with simple molecules like O_2, H_2, NO and CO. Thereafter, in Section 3.3, we go a step further and will consider the effect of mixtures of gases, thus alloys under catalytic turnover. The DFT calculations cited in following sections employ the generalized gradient approximation (GGA) for the exchange and correlation functional, using either the PBE,[31] revPBE[50] or RPBE[51] parametrization. For more details please refer to the original papers.

3.2.1. Bulk, surface and near surface single- and poly-crystalline alloys. Although typical surface science experiments frequently focus on well defined single crystals, *in situ*, elevated pressure studies over single crystalline alloys, compared to supported nanosized particles (see below), are rather limited. Nevertheless, extended bulk materials offer a great opportunity for model studies. The AuNi surface alloy is one of the most prominent examples of the so called "rational catalysts' design"[15] and at the same time demonstrates the significance of the so-called 'pressure gap' effect on surface studies. Combining DFT and atomic resolution STM under vacuum, Besenbacher *et al.* showed that in contrast to the predictions of the bulk phase diagram, Au and Ni can form a quite extended surface alloy, which is equally active, but less prone to deactivation compared to pure Ni.[15] However, some years later, the same group using high-pressure STM showed that the AuNi surface alloy is stable only under UHV conditions or Langmuir CO exposures, while higher CO pressure induces dealloying (phase separation) and formation of monoatomic Au islands over nickel, even at room temperature.[52] The rate of dealloying process is directly related to the CO pressure above the sample (Fig. 4). At CO pressure of 1000 mbar the effect was rapid, while at 7–53 mbar it was much slower and the authors were able to follow the dynamics of the de-alloying process by acquiring STM movies (sequential fast acquisition of STM images). DFT calculations revealed that formation of volatile Ni-carbonyl species at kink-sites was mainly responsible for the observed de-alloying.

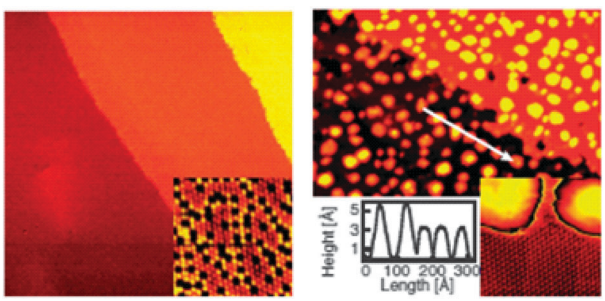

Fig. 4 (a) STM image (800 × 800 Å^2) of Au/Ni(111) after annealing (alloy formation). Inset: atomic-resolution image (50 × 50 Å^2) of the Au/Ni(111) surface alloy. The Au atoms are imaged as depressions. (b) STM image (1000 × 1000 Å^2) of Au/Ni(111) after exposure to 1000 mbar of CO, in which case the surface is observed to be covered with islands. The line scan (indicated by the white arrow) shows islands of two different heights. Inset: atomic resolution of an area between the Au islands (60 × 60 Å^2) reveals a clean Ni(111) surface. Reproduced with permission from ref. 52.

However the effect was reversible and annealing in UHV at 800 K restored back the initial AuNi surface alloy structure.

Recently, Andersson *et al.*[53,54] demonstrated in two successive publications that the expected (based on thermodynamic concepts) gas-induced surface segregation of the more reactive alloy component might be not always the case. The authors investigated the stability of CuPt near surface alloy (NSA) upon exposure to CO and O_2 environments. The CuPt NSA was prepared by physical vapour deposition of one atomic layer of Cu on Pt(111) and annealing in UHV at 800 K. Combining PES, low energy electron diffraction (LEED) and ion scattering spectroscopy (ISS) techniques the authors showed that in vacuum Cu was preferentially located to the second layer leaving a monoatomic Pt 'skin' at the outermost surface (NSA). Upon Langmuir CO exposures at low temperatures the NSA alloy remained practically intact. In contrast, after treatments in 2 mbar CO at temperatures between 473 and 723 K, the initial surface configuration was modified in a rather unexpected way. Copper was segregated to the surface and formed a stable self-organized CuPt surface alloy, on which the CO bond strength was higher compared to the pure Pt(111) surface. Since CO bonding to pure Pt is stronger compared to pure Cu surfaces, segregation of Cu upon CO exposure contradicts at a first glance to the thermodynamic expectation for surface segregation of the more reactive surface component (in this case Pt). However, by using DFT calculations, the authors could rationalize their experimental findings showing that the Pt–CO bond energy considerably increases in the presence of Cu in the first surface layer. By exposing CO–PtCu to 200 mbar of O_2, CO is removed and an ultra-thin CuO_x film is built up on the surface. This process is reversible and the surface alloy is reformed upon re-exposure to CO.[54]

In contrast to CuPt, adsorbate-induced surface segregation of the PtFe NSA showed a rather conventional behaviour when tested under 1×10^{-6} mbar of O_2 and H_2.[55] The PtFe NSA prepared in UHV over the Pt(111) crystal consists of a Fe subsurface layer under the Pt skin. Exposure to O_2 at 850 K induced surface segregation and oxidation of Fe to FeO. As in the case of CuPt, this process is reversible and in H_2 FeO is reduced back to Fe and dilute into the subsurface forming a NSA similar to UHV conditions. By DFT calculations it was confirmed that subsurface Fe was thermodynamically more stable in UHV and H_2 environments, while in O_2 the significantly stronger Fe–O bond, compared to Pt–O, was responsible for Fe segregation over Pt. Similarities of the PtFe surface termination between reducing gas atmospheres and acidic electrochemical environments can be derived. By using *in situ* electrochemical STM, Wan *et al.*[56] observed the formation of a Pt skin layer with pronominally (111)-oriented facets on the surface of Pt–Fe alloys under potential cycling in 0.1 M $HClO_4$ solution. In contrast to H_2 gas exposure, where Pt surface segregation was due to Fe subsurface diffusion,[55] in acidic electrochemical environments the formation of Pt-skin layer is caused by the dissolution of Fe into the acidic solution.[56]

Apart from single crystalline surface and near-surface alloys, polycrystalline bulk Pt–M (M = Sn,[57] Ni[58] and Co[58,59]) alloys have been studied upon exposure to O_2 and H_2 environments. In all the above cases surface segregation of Pt was observed in H_2, while in O_2 segregation and oxidation of the other alloy constituent

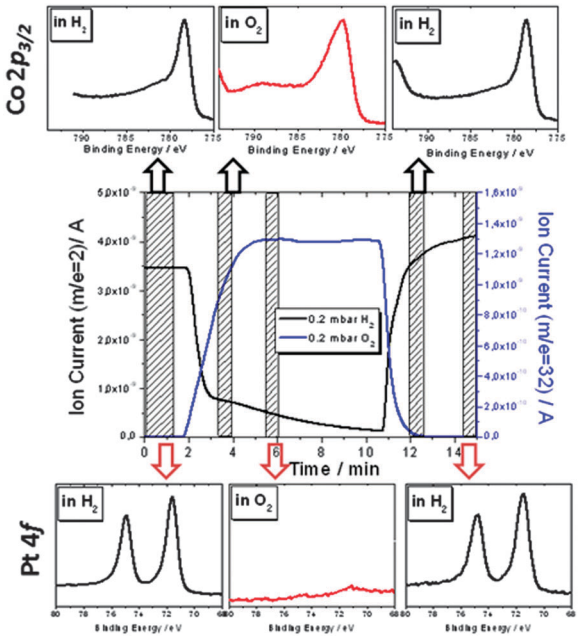

Fig. 5 Real-time experiment showing the evolution of Co $2p_{3/2}$ (top) and Pt 4f (bottom) spectra from a PtCo polycrystalline foil in response to the changes of the gas atmosphere in the experimental cell. The on-line mass spectrometry signal for O_2 and H_2 and the periods of photoemission spectra acquisition are shown in the central diagram. The total gas pressure and the temperature were kept constant at 0.2 mbar and 520 K, respectively. Reproduced with permission from ref. 59.

were found. By using real-time APPES, Papaefthimiou *et al.*[59] have shown that extended segregation on the PtCo bulk alloy takes place within seconds in response to the gas phase environment (Fig. 5). A thick (>5 nm) Co_3O_4 oxide layer is formed over Pt in 0.2 mbar O_2 at 520 K. This effect was reversible, and in H_2, reduction of Co_3O_4 followed by re-segregation of Pt and bimetallic PtCo surface was observed. Surprisingly for a bulk alloy, Pt did not have a notable effect on the reduction process of cobalt oxides. This was rationalized based on the observation that Pt was well diffused in the interior under oxidizing conditions and during reduction it reappeared on the surface only shortly after cobalt has reverted to the metallic state.

Compared to Au and Pt-based alloys, segregation in alloys containing two or more transition metals is in general more difficult to categorize since their oxygen affinity is usually high and similar, while formation of mixed oxide phases might complicate their behaviour. Oxidation of Cu_3Fe,[60] $Cu_{2.75}Ni_{0.25}Fe$,[60] $Ni_{65}Nb_{35}$[61] and NiCo[62] polycrystalline alloys has been studied by surface sensitive methods. As shown by *in situ* APPES and XANES studies, the surface of Cu_3Fe alloys is not significantly influenced by exposure to 1 mbar O_2 or H_2 at 527 K. In contrast, formation of a ternary alloy by Ni addition significantly enhances Fe and Cu reduction in H_2 and promotes segregation of metallic Cu. The presence of Ni also found to hinder re-oxidation of the alloy constituents upon O_2 annealing.[60] The surface composition of $Ni_{65}Nb_{35}$ polycrystalline alloy upon exposure to 1 bar of O_2 is temperature dependent. In particular, up to 373 K, Nb segregates and forms Nb_2O_5, while above 523 K segregation of nickel as a mixture of metal and oxide is observed.[61] The temperature dependence of the oxidation

mechanism was attributed to the different kinetics in the diffusion of constituent atoms. It is interesting to note that the bulk structure of the alloy was not influenced in the course of the experiment. In a recent study of NiCo alloy oxidation, a clear effect of the pressure gap was observed.[62] At low oxygen pressure (10^{-6} mbar), segregation and preferential oxidation of cobalt to CoO take place, while oxidation of nickel is largely suppressed. At ambient O_2 pressure, alloy oxidation was temperature dependent (as in the previous case of NiNb). Up to 520 K, cobalt segregated to the surface and transformed to CoO, similar to the observations at low pressure O_2 exposure. However, at higher temperatures, nickel re-segregates to the surface, at the expense of cobalt, while the remaining CoO is further oxidized to Co_3O_4. In this temperature range, formation of mixed Ni–Co–O spinel-like oxide was proposed based on experimental evidence.

Pd and Rh are typical elements of automobile exhaust catalysts and therefore studies of their redox behaviour might have major technological and economic impact. Bulk PdRh alloy has been studied by Grass *et al.* in various oxidative (O_2, NO) and reducing (CO, H_2) atmospheres using APPES.[63] As in the cases of NiNb and NiCo, a notable effect of the annealing temperature to the surface state was observed. At temperatures below 473 K the surface oxidation state could be controlled by the redox potential of the gas phase but without significant surface segregation effects. In contrast, at high temperatures (623 K) modification of the oxidation state is followed by prominent surface reorganization. Segregation of Rh over Pd was favoured at oxidative environments, and *vice versa* in reducing environments. In this study a comparison between the behaviours of extended and nanosized alloys with the same nominal composition was attempted. Segregation and oxidation/reduction were found to proceed faster at lower temperatures for nanosized alloys compared to the extended bulk materials.

3.2.2. Micro- and nano-sized supported alloy particles. In the case of supported alloy particles, surface segregation might be complicated by preferential bonding of one of the alloy constituents with the support at the metal–support interface. Therefore the interaction between the metals and the support is of major importance for the stability and the chemical activity of the interfacial sites. In the last few years, reduction and oxidation of several Pt-based supported bimetallic nanoparticles have been studied by *in situ* methods. Somorjai and co-workers systematically studied restructuring of supported bimetallic nanoparticles in oxidizing and reducing environments, mainly by ambient pressure photoelectron spectroscopy.[23,64] In that direction, $Rh_{0.5}Pd_{0.5}$ and $Pt_{0.5}Pd_{0.5}$ nanoparticles (diameter 15 ± 2 nm) supported on SiO_2/Si wafers were synthesized by colloidal chemistry methods.[64] The as-synthesized nanoparticles (NPs) had a core–shell structure with a Rh-rich surface for RhPd and a Pd-rich surface for PtPd, respectively. Depth dependent APPES experiments under 0.1 Torr of oxidizing (NO or O_2) and reducing (CO or H_2) environments at 573 K indicated that RhPd readily responded to the surrounding gas phase. In particular, Rh oxidizes and segregates to the surface in NO or O_2, while in CO or H_2, reduction of Rh_xO_y induces Rh diffusion into the core and the formation of a Pd rich surface. The oxidation state of Pd was not significantly influenced by the gas environment and it remained partially oxidized. In contrast, when Pd was alloyed to Pt to form particles with similar sizes to RhPd, the Pd oxidation state changed in response to the gas environment, but no obvious segregation was found. This is a clear indication that modification of the oxidation state does not always follow by surface reorganization.

Since the maximum pressure at which the APPES technique can operate is limited to a few mbar, in a more recent work *in situ* XANES was used to monitor the oxidation state of 4 nm PtCo NPs deposited on a Au foil, at pressures up to 1 bar of O_2 and H_2.[23] It was found that Pt catalyses the reduction of cobalt oxides in H_2, while under O_2 the effect of Pt on the cobalt oxidation state is pressure dependent. A stable tetrahedral Co^{2+} oxide was found coexisting with the octahedral Co^{2+} phase. In another study, the redox behaviour of 3 nm PtCo NPs prepared by physical methods (Low Energy Cluster Beam Deposition technique) and deposited on amorphous carbon was studied by a combination of APPES and XANES techniques.[59] For comparison, a polycrystalline PtCo foil was measured under the same conditions in order to reveal size dependent effects. It was shown that Pt segregation took place in 0.2 mbar H_2, while segregation and oxidation of cobalt were evident in 0.2 mbar O_2. The presence of tetrahedral Co^{2+} species (being metastable as bulk phase) was confirmed by theoretical simulations of XANES peaks and it was also affirmed that its stability was related to the size, since it was not observed in the bulk samples under identical conditions. Comparison with reference monometallic cobalt samples indicated that the promotion effect of Pt to the reduction of the surface cobalt oxides is mainly pronounced in nanosized samples, while for the bulk polycrystalline foil, Pt does not markedly influence the reduction of Co oxides. However, in contrast to the findings on the PdRh[63] system, nanosized PtCo was more difficult to reduce compared to the extended PtCo bulk alloy. The essential advantage of physical preparation methods used in ref. 59, compared to chemical synthesis typically employed in nano-alloys redox studies, is the capability to synthesize bare (uncoated) nano-objects well suited as model systems for fundamental studies. In contrast, using chemical synthesis methods the surface of the prepared NPs is affected by the interaction with the solution molecules, which in turn might also influence the redox behaviour.

In a much earlier investigation nanosized PtCo supported on SiO_2 and prepared by spin coating method was studied by *in situ* XANES[65] under 1–2 mbar H_2. AFM images indicated relatively flat, around 2 nm thick, PtCo layers. It was suggested that the as-prepared fresh film consisted mainly of octahedral Co^{2+} species (however a comparison with recent results[59] indicates that the Co L-edge resembles more tetrahedral Co^{2+}), while formation of PtCo alloyed bimetallic particles was observed after reduction in H_2. It is noteworthy that compared to the relatively inert Au and carbon supports employed in ref. 23 and 59, respectively, SiO_2 might have a greater influence on the reduction of PtCo NPs. Apart from gas atmospheres, surface segregation of carbon supported PtCo NPs (sizes around 5 nm) was also investigated under electrochemical environments.[66] An interesting comparison between samples treated in gas-phase and alkaline electrochemical environments was attempted by an *in situ* cycling voltammetry

(CV) method. Both, ambient pressure CO exposure at 473 K, and potential cycling in the CO-saturated alkaline electrolyte, lead to the same Pt core–Pt_xCo_y shell structure. It should be noted that cyclic voltammetry is extremely sensitive to the outermost surface layer, however the interpretation of the current–voltage plots is not straightforward and other analytical techniques should be employed complementary to CV in order to elucidate the surface structure.

Apart from PtCo, surface segregation in reducing and oxidizing environments of other Pt based supported bimetallics (Cu,[67,68] Sn,[69] Rh,[70,71] Ni[67] and Au[72,73]) has been studied. The surface structure of Al_2O_3 supported 2.5 nm PtCu nanoparticles was found sensitive to the type of reducing gas. By combing X-ray absorption (XANES), pair distribution function analysis (PDF) and Fourier Transformed infrared spectroscopy (FT-IR) in ambient H_2 pressure (548 K), no core–shell structure formation was observed, but the NPs surface was enriched in Cu, while in the interior, alloy PtCu remained.[68] An inverse observation was found in ambient pressure CO exposure (up to 623 K) where Pt segregation with subsequent migration of Cu in the core took place.[68] This study could not confirm Cu segregation in CO atmospheres observed on single crystalline PtCu NSA.[53] This indicates that support and size effects are of major importance to the surface segregation phenomena. Nanosized PtCu and PtNi were supported on Highly Ordered Pyrolytic Graphite (HOPG) and they were characterized by XPS after 1 bar of H_2 or O_2 treatment at 573 K in a reaction cell attached to the UHV set-up.[67] Similarly to PtCo, Cu and Ni were oxidized and segregated to the surface in oxidative atmospheres, while in H_2 the surface was enriched in Pt. The redox kinetics of Pt_3Sn alloy NPs (mean size 15 nm) supported on Al_2O_3 was studied by *in situ* time-resolved energy dispersive XAFS (DXAFS) and quick XAFS (QXAFS).[69] Oxidation at 673 K under atmospheric O_2 pressure was found to proceed in 3 steps: (a) a fast step of Pt_3Sn transformation to SnO_2 shell–Pt core structure, (b) oxidation of the surface of Pt–core to PtO and (c) finally these transformations were followed by shape restructuring of the nanoparticles (Fig. 6). Reduction in H_2 at the same temperature proceeds in one step and regenerates the initial Pt_3Sn alloy.

The effects of size and morphology of MgO supported PtRh to the oxidation process were studied by scanning photoelectron microscopy (SPEM) and low energy electron microscopy (LEEM).[70] Independently from the particle size, a thick Rh-oxide layer with various Rh stoichiometric oxide phases was formed, whereas oxidation of Pt was limited to the top few atomic layers. It was also found that the degree of oxidation within a single microparticle is not homogeneous and correlates to the initial microstructure of these particles. The Pt and Rh oxidation states were systematically higher as the size of the PtRh aggregates decreased. Oxidation of PtRh alloys is not only influenced by the size but also by their composition. In particular, $Pt_{0.9}Rh_{0.1}$ and $Pt_{0.95}Rh_{0.05}$ supported on Al_2O_3 catalysts with mean particle size around 2 nm were annealed in 0.7% NO in N_2 up to 473 K and their surface state was indirectly characterized by FT-IR using NO as a probe molecule. Both surfaces contained a mixture of oxidized Pt and Rh species, however the amount of surface Rh oxide was directly related to its nominal content.[71]

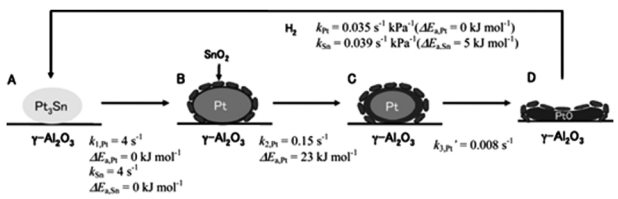

Fig. 6 Proposed mechanism for the oxidation and reduction of Pt–Sn nanoparticles on γ-Al_2O_3. The kinetic parameters were determined by the time-resolved XAFS. Reproduced with permission from ref. 69.

Tenney and coworkers investigated Pt–Au[73] and Ni–Au[72] nanoparticles supported on TiO_2(110). They found that under Langmuir CO exposure, segregation of Ni and Pt on the surface occurred, whereas under UHV, Au is preferentially segregated over Pt and Ni. For PdAu bimetallic particles supported on TiO_2 no evidence was found for any surface segregation upon annealing at 548 K in ambient pressure H_2,[68] however when the gas atmosphere was switched to CO, adsorbate induced surface segregation of Pd was observed. CO adsorption on PdAu bimetallic surfaces was recently addressed by Garcia-Mota and Lopez by DFT (RPBE functional) and they calculated also IR frequencies of adsorbed CO for a high number of possible configurations.[74]

IrNi core–shell nanoparticles (2.2 to 3.4 nm) supported on high area Vulcan carbon were found to form an Ir shell–IrNi core structure upon annealing at 873 K at ambient pressure H_2.[75] This catalyst was tested in an acidic electrochemical environment and found to be stable under elevated potentials (up to 1.11 V with respect to the reversible hydrogen electrode), since nickel atoms in the core were protected against oxidation and dissolution into the acidic media.

Formation of surface alloys under reactive conditions has been also observed for non-typical bimetallic systems, like oxide supported metal catalysts. Strong indications of a surface CuZn alloy was given by the group of Topsoe *et al.*[76,77] during annealing of Cu/ZnO methanol synthesis catalysts. Exposure to strong reducing gas phases (CO and H_2) at medium temperatures (500 K) induces reduction of ZnO and migration of Zn to the Cu surface where a surface CuZn alloy is formed. This procedure was found to be reversible and Cu/ZnO was re-established upon exposure in oxidative atmospheres.

3.3. Catalytic systems

In the following section, we are going to review selected systems of alloy catalysis in which segregation or phase separation has been reported.

3.3.1. CO oxidation. CO oxidation is one of the more simple and generic heterogeneous catalytic reactions, with some interest in both applied and academic research. Its popularity has been additionally fuelled by the promise to apply CO oxidation as a model reaction to understand issues surrounding the pressure and material gap often observed when attempting to transfer knowledge from basic surface science to real world catalysis and *vice versa*. It was early recognized that alloy catalysts hold promise to find active and stable catalysts for this reaction. It has been shown regularly

and will be discussed here that this is essentially related to the different requirements for activating O_2 and CO.

As we have discussed above, $Rh_{0.5}Pd_{0.5}$ bimetallic Pd-core Rh-shell nanoparticles undergo significant changes in the surface composition when exposed to CO, O_2 and other gases.[64] However, reducing gases, such as CO, interacted with Pd more strongly inducing its segregation to the surface, whereas oxygen (or oxidizing gases such as NO) reversed this trend. Rh_xPd_{1-x} bimetallic catalysts exhibit the synergetic effect of increased reactivity compared to pure Pd or Rh in CO oxidation by O_2 or NO.[78,79] Stronger activity enhancement is observed when oxygen is in excess of CO. Segregation phenomena, again studied using APPES, have massively slowed down in CO oxidation due to the opposite effect of CO and O_2. Nevertheless, it was shown that higher temperature and lower oxygen excess result in higher Pd surface concentration. Both Pd and Rh are mainly metallic, with a minor oxidized Rh component, but at a higher pO_2/pCO ratio more RhO_x is formed. Due to the preferential adsorption of CO on (isolated) Pd sites and the activation of O_2 over Rh/RhO_x, the synergetic effect of bimetallic PdRh is attributed to a bifunctional mechanism with emphasis on the Pd–RhO_x interface where oxygen spillover from Rh to Pd sites assist the reaction.

AuPd alloy materials catalyze the synthesis of vinyl acetate, H_2O_2, selective oxidation of alcohols but also can diminish CO emission. In a series of publications, Goodman and co-workers have studied by PM-IRAS the reasons behind the enhanced reactivity of AuPd in CO oxidation.[80–83] They find that well-annealed samples with low surface Pd content are essentially inactive at low pressures, whereas higher pressures facilitate the reaction. These latter conditions are linked to higher CO and O coverages enabling the segregation of Pd to the surface.[84–86] Segregation of Pd was found to be O coverage dependent with more than 1/3 of the monolayer being necessary to induce segregation,[86] whereas CO pressure in the range of 10^{-3} Torr was enough to induce Pd segregation and 10^{-1} Torr to form contiguous Pd sites.[80,82,84] Once segregated to the surface, due to the weak interaction, Pd sites do not have the tendency to cluster,[85] and thus there is need of higher pressure to make Pd pairs. By following the carbonyl stretching vibration *in situ*, Goodman deduced a link between the presence of contiguous Pd sites and the reactivity. Apparently, neither Au nor isolated Pd sites were capable of dissociating O_2, and the reaction only occurred once adsorbate induced surface segregation reached a level of forming contiguous Pd sites. They also noted that CO can adsorb on both Au and Pd sites weaker than on monometallic Pd. These observations in conjunction with the higher reactivity and lower apparent activation energy in comparison to the monometallic Pd counterpart are attributed to a mechanism where CO inhibition does not occur and CO and O_2 activation is separated on the alloy surface. It is interesting to note that AuPd was less prone to surface Pd oxidation and thus to deactivation. Somewhat differently from the results above, Alayoglu *et al.*[87] reported that Au_xPd_{1-x} nanoparticles (8–11 nm; $x = 0.25, 0.5, 0.75$) synthesised at low temperature (500 K) with poly(vinyl-pyrrolidone) surfactant are enriched in Pd at the surface, but also show higher turnover rates than the parent monometallic nanoparticles. Alloy particles with 75% and 50% nominal Pd content have not shown any significant changes in the surface composition upon CO oxidation at 473 K. On the other hand, $Au_{0.75}Pd_{0.25}$ nanoparticles restructure irreversibly to Au-rich surfaces in the reaction. The authors explained this unexpected finding by the higher gain of energy (lower surface energy of Au) with Au segregation than the gain of reactant adsorption on Pd sites.

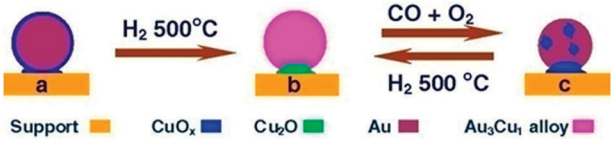

Fig. 7 Schematic illustration of the structural changes of the Au–Cu/SBA-15 under H_2 reduction and CO oxidation conditions. Reproduced with permission from ref. 88.

AuCu bimetallic nanoparticles supported on the mesoporous aluminosilicate SBA-15 have been reported to be highly active in CO oxidation below RT. Using multiple *in situ* techniques (XRD, FT-IR, XANES) Liu *et al.* investigated this catalyst under activation and reaction.[88] They observed that the as-calcined catalyst was made up of a gold core decorated with CuO patches (Fig. 7). During the activation at 773 K, a part of CuO was reduced to Cu and diffused into the core forming an Au_3Cu_1 intermetallic phase, whereas the other part of CuO that was interacting with the support was only reduced to Cu^+ acting as "nano-glue" between Au_3Cu_1 particles and the support. During CO oxidation Cu segregated from the intermetallic core to the surface forming tiny CuO_x patches over Au, and so, producing an intimate contact with long perimeter between gold and CuO_x. CO adsorbed on metallic gold sites was deduced to react with activated oxygen provided by the neighbouring oxidized copper sites.

Applying *in situ* Mössbauer and FT-IR spectroscopy, Margitfalvi *et al.* studied a $SnPt/SiO_2$ catalyst (Sn/Pt = 0.68) active in low temperature CO oxidation.[89] They found that activation in hydrogen (573 K) resulted in two bimetallic phases, while oxidized species were absent. During CO oxidation at RT, the alloy phases segregated into a PtSn (1 : 1) phase with additional two types of oxidized Sn^{4+} species. Pure CO produced no measurable bridged carbonyl band in the IR spectrum; however addition of oxygen induced the appearance of subtle but continuous growth of tiny bridged CO. It was concluded that the *in situ* formation of Sn^{4+}–Pt ensemble was the key feature of this catalytic system.

In a first principle study, Su *et al.* investigated the structural changes of Pt-3d transition metal (Cr, Mn, Fe, Co, Ni and Cu) alloys under reductive and oxidizing conditions as well as in CO oxidation.[90] Under reductive conditions (vacuum or CO) the 3d transition metal was shown to prefer subsurface sites and avoid surface sites because of its higher surface energy and smaller atomic size. On the other hand, in oxidizing conditions employing 0.25 ML O coverage, the strong interaction between the surface oxygen and the 3d metal (with the exception of Cu) induces the migration of 3d metal to the surface, which may even form oxidized 3d transition metal islands. This indicates, but also additional calculations have confirmed, that exposed 3d sites are highly facile for molecular oxygen dissociation. Therefore, enhanced CO oxidation activity can be achieved on Pt-3d transition metal ensembles, where CO adsorbs on Pt sites and O_2 activation occurs on dispersed and partially oxidized 3d atoms. Overall reactivity is therefore very

high, as CO poisoning, relevant on sole Pt surfaces, does not affect this Pt-3d system. In this respect it is interesting to mention that eliminating atomic oxygen from AuNi can also be a difficult step.[91]

3.3.2. Other reactions with CO. AuPd(100) catalyzes the CO + NO reaction with higher turnover rate and enhanced N_2 selectivity than does monometallic Pd.[81] Since the kinetics was somewhat similar to CO oxidation and increasing pressures resulted in increasing reaction rate, as well as enhanced Pd segregation with the formation of contiguous Pd sites, the authors derived essentially the same conclusion, as we have discussed above, namely that NO (as O_2) activation requires contiguous Pd sites. The lower CO binding energies with the alloy surface provided a fair amount of empty ensembles for NO dissociation at low temperature facilitating the reaction. It was also found that low doses of NO promote the CO + O_2 reaction, likely by NO_2 formation that dissociates more easily than does O_2. The $Rh_{0.5}Pd_{0.5}$ nanoparticles have been also studied by APPES in the CO + NO reaction at 573 K,[64] and the conclusions reached resemble well those in CO + O_2 case: the oxidized Rh shell gets reduced (with remaining ~20% oxidized Rh) and Pd segregates to the surface. The difference is that somewhat higher Pd surface concentrations (~50%) are reached and Pd is also partially oxidized (Fig. 8).

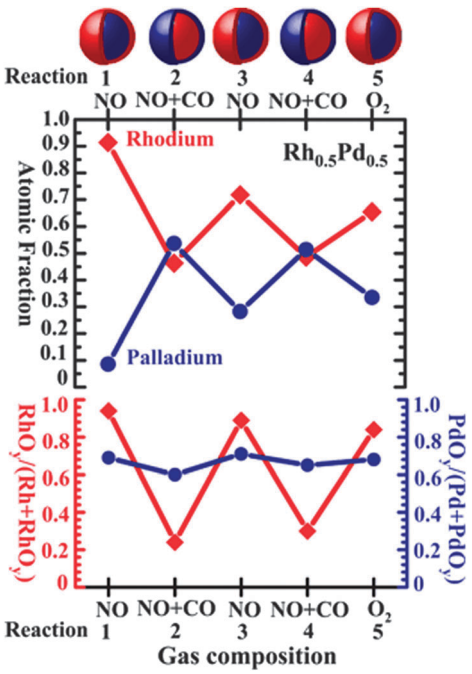

Fig. 8 (Top) Evolution of Rh (Rh^0 + Rh^{2y+}) and Pd (Pd^0 + Pd^{2y+}) atomic fractions in the $Rh_{0.5}Pd_{0.5}$ NPs at 300 °C under oxidizing conditions (100 mTorr NO or O_2) and catalytic conditions (100 mTorr NO and 100 mTorr CO) denoted in the *x*-axis. (Bottom) Evolution of the fraction of the oxidized Rh (left *y*-axis) and Pd atoms (right *y*-axis) in the examined region under the same reaction conditions as the top part of the figure. All atomic fractions in this figure were obtained with an X-ray energy of 645 eV for Rh3d and Pd3d, which generates photoelectrons with a mean free path of ~0.7 nm. Schematic diagrams above the top of the figure show the reversible segregation of Rh and Pd under alternating oxidizing and catalytic conditions. The *y*-axis data points for reactions (1), (3), and (5) have an associated error of ±0.03; for reactions (2) and (4), the error bar is ±0.02. Reproduced with permission from ref. 64.

Andersson *et al.*[53,54] after establishing that adsorbate CO may pull the least reactive alloying component Cu to the surface whereas Pt, the other alloy component, in this way forms a much stronger bond with CO, has investigated the stability of this surface structure in various gas mixtures (CO + H_2O or CO + H_2) using PM-IRAS. No indication of substantial changes in surface structure was found under these conditions (up to 673 K) compared to CO alone in the gas phase. On the other hand, O_2 at 200 mbar pressure and RT was capable to remove the carbonyl band and build up an ultra-thin CuO_x film.

Anderson *et al.*[92] investigated zeolite supported PdCu bimetallic catalysts and by applying XANES in the hard X-ray regime and FT-IR experiments under CO hydrogenation at reaction temperature examined how the surface and bulk phase were influenced by the reaction condition. While XANES indicated that only one type of substitutionally disordered PdCu alloy phase was formed and stayed unmodified under longer periods at reaction conditions, FT-IR suggested that adsorbate induced surface segregation of Pd occurred. Despite Pd segregation, a progressive loss of Pd threefold adsorption centers was observed as a function of time on CO hydrogenation stream.

3.3.3. Methanol steam reforming and water gas shift reactions. Methanol steam reforming (MSR) producing H_2 and CO_2 (without significant CO selectivity) is one possible technology for on-board hydrogen generation to feed fuel cells. Besides the Cu/ZnO system, Pd/ZnO was identified as a promising catalyst.[93] Pd on inert, non-reducible support catalyzes methanol decomposition to CO and H_2, and thus with the Pd/ZnO system the active role of PdZn intermetallic compound has been speculated. Combining X-ray absorption spectroscopy with on-line activity measurements, Föttinger *et al.*[94] examined a 7.5 wt% Pd/ZnO catalyst and its dynamic changes occurring upon various treatments and MSR conditions. The PdZn alloy phase was unambiguously identified forming in the early stage of reaction at 623 K that changed the reaction selectivity from methanol decomposition to steam reforming. Alloying was assumed to occur *via* hydrogen that has been generated in methanol decomposition, spilling over to and reducing the support. Alloying steadily increased with time on MSR in forming a thicker alloy shell on the Pd particles. Oxygen treatment resulted in phase separation (Pd and ZnO formation); nevertheless alloy formation is reversible as repeated reaction runs allowed the reformation of the alloy phase with concomitant increase in MSR selectivity. Rameshan *et al.*[95,96] deduced from model catalyst studies under *in situ* MSR conditions that a "multilayer" (*ca.* five layers) PdZn 1 : 1 near-surface alloy exhibits high CO_2 selectivity, whereas a monolayer PdZn 1 : 1 surface alloy, despite its identical surface composition, produced only CO and H_2.

Pt-based binary and ternary systems may eliminate CO poisoning of fuel cell anode electro-catalysts. Zafeiratos *et al.*[97] studied the methanol steam reforming reaction (MSR) in conjunction with the water gas shift (WGS) reaction over a ternary PtRuCo alloy catalyst using APPES, with the aim to identify the nature of the working catalyst surface and thus providing a basis for the role of promoters. The surface of PtRuCo catalyst

undergoes significant modifications in its composition and chemical state in response to the reaction mixture. Under MSR reaction conditions Pt, Ru and Co were metallic with traces of ionic Co^{x+} also observed. Significant amounts of adsorbed carbon and oxygen species were attached to the surface and indications of sub-surface (dissolved) oxygen were also found. Rich in water WGS mixtures favour surface oxidation reflecting the higher oxygen chemical potential compared to the MSR mixture and induced surface reorganization. In particular, cobalt segregates to the surface and is, to a large extent, oxidized during WGS. Interestingly, traces of ionic Pt species were also observed, while Ru was mainly metallic. Compared to MSR reaction less carbon and more surface oxygen species were observed. A bifunctional active site complex with possible electronic contribution was put forward to explain the function of the material. Additional experiments with a polycrystalline $Pt_{0.5}Co_{0.5}$ foil sample under MSR indicated the formation of Pt-skin, cobalt-rich subsurface and Pt-rich core structure with carbon and oxygen based adsorbates and dissolved oxygen.

3.3.4. Hydrogenation reactions. For selective hydrogenation of multiple unsaturated compounds, high-performing heterogeneous catalysts mainly consist of multi-metallic systems facilitating increased selectivity. These materials, however, often undergo segregation phenomena and thus, in order to understand their structure-function relation, a surface sensitive *in situ* methodology is essential. Palladium, a typical hydrogenation metal, alloyed with Ag, Au or Cu has often been investigated, and first we focus our attention to these catalysts.

Pd surface segregation reportedly occurs at the high hydrogen pressure side of a PdAg membrane.[98] Using density functional calculations, Gonzalez *et al.* studied the surface structure of a $Pd_{0.8}Ag_{0.2}$ alloy and its modification in the presence of atomic hydrogen.[99] At equilibrium and in complete absence of adsorbates, the surface is predicted to expose mostly silver atoms, as discussed above. Increasing the coverage of adsorbed H atoms from 1/9 to 4/9 ML gradually decreases the energy gain of lower Ag surface energy, suppresses the surface segregation of Ag, and migration of all silver surface atoms into the subsurface region becomes favourable at a H coverage of $\sim$0.25 ML. For this Pd-skin structure with predominantly Pd atoms in the surface layer and Ag below, the propensity of H to accommodate interstitial sites below the surface vanishes. In this regard, it is interesting to mention that Teschner *et al.*[100,101] has shown that during selective alkyne hydrogenation over monometallic Pd catalysts the subsurface interstitial sites are carbon populated, carbon being absent under nonselective reaction. Later, using DFT calculations, it has been established that subsurface carbon decreases the binding energy of adsorbed H, forms an exclusion zone for subsurface H and increases the barrier for bulk dissolved hydrogen diffusing to the surface; all these contributing to a low surface H concentration essential to avoid over-hydrogenation.[102] Selectivity is also often enhanced with addition of CO to the feed, which was shown by adsorbing strongly on Pd to diminish subsurface and bulk H population and enable only low surface hydrogen concentration.[103]

The Pd pseudomorphic monolayer on silver has been shown recently to decrease the formation of both C and H in the subsurface.[104] A somewhat different role of silver was suggested by Jin *et al.*[105] proposing the dilution of surface Pd sites by Ag being important for improved acetylene hydrogenation selectivity. Similar improved selectivity in 1,3-butadiene hydrogenation was observed over palladium catalysts alloyed with gold.[106,107] $Pd_{0.7}Au_{0.30}$ single crystal surface after vacuum annealing is strongly enriched by gold.[106] Di Vece *et al.*[108] observed changes in the size distribution and composition of bimetallic PdAu nanoparticles that have been exposed to hydrogen at RT. The effect was identified to be due to Ostwald ripening of Pd after Pd has segregated to the surface. An increased reactivity with time on stream in butadiene selective hydrogenation was attributed to adsorbate induced partial Pd segregation to the surface.[106] Interestingly, Hugon *et al.*[107] observed no comparable change in the activity of a PdAu catalyst (Au/Pd = 10), despite detecting Pd segregation in separate CO adsorption FR-IR experiments.

Very recently, Lopez and Vargas-Fuentes reviewed the role of metallic promoters in Pd-based alkyne hydrogenation and presented new insights from their DFT calculations regarding stability and segregation, adsorption properties, and the ability to form hydride and carbide phases.[109]

In hydrogenation chemistry, up to now we have considered mainly the effect of hydrogen on the segregation properties. Applying medium-energy ion scattering (MEIS), the effect of organic component on segregation has been explored.[110–112] Noakes *et al.*[110] used a $Pd_{0.5}Cu_{0.5}$(110) single crystal, which was slightly Pd-rich under the initial preparation condition. Adsorbing ethylene at 468 K gave rise to substantial Pd segregation. This indicates that both hydrocarbon and hydrogen would induce Pd segregation in Pd catalysts when alloyed with more noble elements like Cu, Ag or Au. On the other hand, if the organic molecule contains more electronegative functional groups, the situation may be reversed, as suggested by the adsorption of trichloroethylene over the same $Pd_{0.5}Cu_{0.5}$(110) single crystal. In this case, Cu enrichment in the first surface layer was shown by MEIS. Baddeley and co-workers using MEIS investigated the adsorption of (*S*)-glutamic acid[111] and methylacetoacetate[112] on bimetallic NiAu surfaces and found in both cases Ni segregation. From the enantioselective methylacetoacetate hydrogenation point of view, Ni segregation around the adsorption site is likely not beneficial. Conversely, if a chiral modifier, such as the (*S*)-glutamic acid, induces Ni enrichment, this can produce more active reaction sites and hence the reactivity can improve. Platinum surfaces, alloyed with electropositive 3d metals, are reported to increase selectivity in the hydrogenation of α,β-unsaturated aldehydes towards the desired unsaturated alcohols. Hirschl *et al.*[113] using spin-polarized DFT calculations studied the adsorption modes of acrolein and prenal on $Pt_{0.8}Fe_{0.2}$(111) and their effect on surface segregation. As should be evident from our discussion up to now, the clean alloy surface is characterized by a strong Pt surface segregation. Nevertheless, the considerably higher aldehyde adsorption energy upon formation of O–Fe bonds can modify the segregation profile and increase the Fe content of the surface layer. As concluded, this has a clear effect on the prevailing adsorption mode and energy of the aldehyde reactant, and thus the reaction selectivity is influenced in the desired direction.

Studt *et al.*[114] performed theoretical screening on a broad space of alloys, and with the help of scaling relations discovered new selective acetylene hydrogenation catalysts based on the

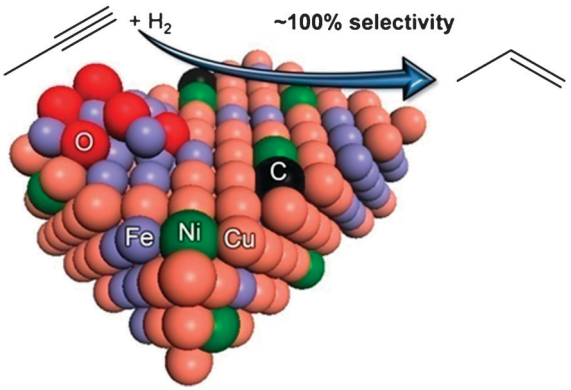

Fig. 9 Schematic view of the surface of $Cu_{2.75}Ni_{0.25}Fe$ under propyne hydrogenation based on *in situ* spectroscopic (XPS/XAS) analyses. Note the depicted surface orientation has no significance here. Reproduced with permission from ref. 60.

nickel–zinc alloy. Recently, Bridier *et al.*[115] identified a novel family of ternary Cu–Ni–Fe catalysts for the partial hydrogenation of propyne with selectivity near 100%. The addition of Ni was the key for the achieved selectivity. In the follow-up work,[60] the surface composition and electronic state of $Cu_{2.75}Ni_{0.25}Fe$ and Cu_3Fe were investigated using *in situ* APPES and XANES to gain insight into the state of the surface and the role of Ni promotion (Fig. 9). The bulk of the calcined samples consisted of CuO as the main phase and $Cu_x(Ni_{1-x})Fe_2O_4$ spinel as the secondary phase, whereas no spinel was identified on the surface, and, instead, Fe_2O_3 was observed. Once the materials were reduced, XRD identified a metallic alloy phase with some Fe_3O_4; nevertheless the surface was still somewhat oxidized containing various oxidized states. Under propyne hydrogenation, the Cu_3Fe surface composed of a Fe-lean alloy phase with additional Fe_3O_4/Fe_2O_3 oxidized surface phases. The surface contained 30% iron but mainly (~90%) in the oxidized form, the alloy was thus very rich in Cu. The surface of reduced $Cu_{2.75}Ni_{0.25}Fe$ was enriched in Cu (~91%), but under propyne hydrogenation both Fe and Ni segregated back to the surface giving rise to near nominal surface concentration. As opposed to the Fe-lean Cu_3Fe alloy surface, most (~70%) of iron in $Cu_{2.75}Ni_{0.25}Fe$ was in its metallic alloy form under hydrogenation. The *in situ* Ni L_3-edge absorption spectra indicated a strong Ni–carbon interaction. It was concluded that Ni not only enhances the surface H coverage, as expected from the low selectivity towards oligomerization, but drastically changes the surface composition. Ni enhances Cu and Fe reduction, thus giving rise to well-diluted Cu surface sites, and hinders re-oxidation that would favour Fe segregation.

4. Conclusions and outlook

Surface segregation under reactive environment is usually underestimated in many of the catalytic studies. Typically, when *in situ* techniques are used, they are often not sensitive enough to the surface, or the surface sensitive methods are only applied *ex situ* (usually postmortem). However, our review illustrates that these effects readily occur, and, as catalysis is a surface event, they are obviously critical. Due to the complexity of the systems (composition of alloys, secondary effects like particle size/support, and external control parameters), segregation and the surface structure are often difficult to predict by general phenomenological models. The pressure and material gap can be very important as shown in many examples, and studies under elevated pressure are essential to establish the surface composition under operating conditions and correlate the surface state to the catalytic performance.

One of the most promising surface sensitive *in situ* tools, APPES, is still confined to few mbar pressures and hence not capable to get utilization at real atmospheric pressure, or above. Clearly, further developments (X-ray source with higher brilliance, more effective electron collection and detection) are required in this respect. New developments and new techniques are essential to go beyond our current understanding, especially related to spatial and temporal resolution during segregation events. Extending the intrinsically bulk sensitive EXAFS towards the surface by implementing modulation excitation spectroscopy and phase sensitive detection[116] may open up new possibilities in studying the structural dynamics of alloy surfaces.

State-of-the-art theoretical treatments, as we have illustrated here, are at least in principle capable to describe the complex interplay of parameters influencing segregation and to predict surface structures under realistic conditions. Once the working state of an alloy surface is established, a standard DFT treatment can be utilized to calculate reaction energy profiles and to perform a microkinetic analysis, thus providing a full picture of a catalytic cycle promoted by a particular alloy. In those systems where the catalytic performance (activity and selectivity) of a material can be rationalized in terms of a universal descriptor (*e.g.* binding energy of one of the intermediates), theoretical methods can be used to quickly screen a large number of alloys and to computationally design new catalysts with improved performance.[117] Clearly, this type of computational screening needs to include the evaluation of stability against segregation and phase separation phenomena.

One needs to keep in mind, though, that catalysis is a non-equilibrium process and the structure of the catalyst surface obtained under the assumption of thermodynamic equilibrium may differ from the one active under reaction conditions. Accounting for these effects requires a full dynamical model of the process, and hence describing the interplay between all the elementary processes (adsorption, desorption, associations, dissociations, *etc.*) involved in the catalytic cycle. Recent advances have brought us closer to this goal through the use of the kinetic Monte Carlo method to simulate the steady state of the catalyst during the reaction, coupled to a first principle description of each elementary step to derive the corresponding rate.[118] This approach has been applied to the oxidation of CO on $RuO_2(111)$ and Pd(100),[119,120] showing that indeed the surface of the catalyst continuously evolves during the reaction cycle, and at the steady state differences from the thermodynamically stable configuration are appreciable.

Alloys have the great advantage to offer access to multi-functional active sites needed for complex reactions and for reactions with selectivity challenges. Moreover, alloys often find application in electrochemical systems, in which, however, surface segregation might be additionally fuelled by selective dissolution of constituents into the liquid phase. Due to the increased difficulty in studying solid–liquid interfaces *in situ*, these

systems are somewhat less understood. Nevertheless, the important challenges we are facing in *e.g.* energy conversion, sustainable production, *etc.* are essentially connected to engineering solid–gas and solid–liquid interfaces to the desired needs. Due to the unlimited possibilities offered by multi-component systems, the rational design of alloys when theory and *in situ* experimentation works hand-in-hand can offer great opportunities.

Acknowledgements

S.Z. gratefully acknowledges financial support from the FP7 Fuel Cells and Hydrogen Joint Undertaking program, under ROBANODE, IRAFC and DEMMEA projects.

Notes and references

1 M. Ni, D. Y. C. Leung and M. K. H. Leung, *Int. J. Hydrogen Energy*, 2007, **32**, 3238–3247.
2 F. Garin, *Catal. Today*, 2004, **89**, 255–268.
3 D. I. Enache, J. K. Edwards, P. Landon, B. Solsona-Espriu, A. F. Carley, A. A. Herzing, M. Watanabe, C. J. Kiely, D. W. Knight and G. J. Hutchings, *Science*, 2006, **311**, 362–365.
4 J. Greeley, T. F. Jaramillo, J. Bonde, I. Chorkendorff and J. K. Norskov, *Nat. Mater.*, 2006, **5**, 909–913.
5 J. Greeley and M. Mavrikakis, *Nat. Mater.*, 2004, **3**, 810–815.
6 J. H. Sinfelt, *Bimetallic Catalysts: Discoveries, Concepts and Application*, Wiley, New York, 1983.
7 J. A. Rodriguez, *Surf. Sci. Rep.*, 1996, **24**, 225–287.
8 N. Toshima and T. Yonezawa, *New J. Chem.*, 1998, **22**, 1179–1201.
9 J. G. Chen, C. A. Menning and M. B. Zellner, *Surf. Sci. Rep.*, 2008, **63**, 201–254.
10 J. R. Kitchin, J. K. Norskov, M. A. Barteau and J. G. Chen, *Phys. Rev. Lett.*, 2004, **93**, 4.
11 O. S. Alexeev and B. C. Gates, *Ind. Eng. Chem. Res.*, 2003, **42**, 1571–1587.
12 R. Ferrando, J. Jellinek and R. L. Johnston, *Chem. Rev.*, 2008, **108**, 845–910.
13 P. Liu and J. K. Norskov, *Phys. Chem. Chem. Phys.*, 2001, **3**, 3814–3818.
14 V. Ponec, *Appl. Catal., A*, 2001, **222**, 31–45.
15 F. Besenbacher, I. Chorkendorff, B. S. Clausen, B. Hammer, A. M. Molenbroek, J. K. Norskov and I. Stensgaard, *Science*, 1998, **279**, 1913–1915.
16 V. Blum, L. Hammer, C. Schmidt, W. Meier, O. Wieckhorst, S. Müller and K. Heinz, *Phys. Rev. Lett.*, 2002, **89**, 266102.
17 J. Nørskov, M. Scheffler and H. Toulhoat, *MRS Bull.*, 2006, **31**, 669–674.
18 C. Stampfl, A. Soon, S. Piccinin, H. Shi and H. Zhang, *J. Phys.: Condens. Matter*, 2008, **20**, 184021.
19 C. Stampfl, M. Veronica Ganduglia-Pirovano, K. Reuter and M. Scheffler, *Surf. Sci.*, 2002, **500**, 368–394.
20 F. Tao and M. Salmeron, *Science*, **331**, 171–174.
21 M. Salmeron and R. Schlogl, *Surf. Sci. Rep.*, 2008, **63**, 169–199.
22 A. Knop-Gericke, E. Kleimenov, M. Haevecker, R. Blume, D. Teschner, S. Zafeiratos, R. Schloegl, V. I. Bukhtiyarov, V. V. Kaichev, I. P. Prosvirin, A. I. Nizovskii, H. Bluhm, A. Barinov, P. Dudin and M. Kiskinova, *Advances in Catalysis*, 2009, vol. 52, pp. 213–272.
23 F. Zheng, S. Alayoglu, J. H. Guo, V. Pushkarev, Y. M. Li, P. A. Glans, J. L. Chen and G. Somorjai, *Nano Lett.*, 2011, **11**, 847–853.
24 A. Christensen, A. V. Ruban, P. Stoltze, K. W. Jacobsen, H. L. Skriver, J. K. Norskov and F. Besenbacher, *Phys. Rev. B: Condens. Matter*, 1997, **56**, 5822–5834.
25 A. V. Ruban, H. L. Skriver and J. K. Norskov, *Phys. Rev. B: Condens. Matter*, 1999, **59**, 15990–16000.
26 Q. Sun, K. Reuter and M. Scheffler, *Phys. Rev. B: Condens. Matter*, 2003, **67**, 205424.
27 N. L. Nguyen, S. Piccinin and S. de Gironcoli, *J. Phys. Chem. C*, 2011, **115**, 10073–10079.
28 D. R. Stull and H. Prophet, *JANAF Thermochemical Tables*, U.S. National Bureau of Standards, Washington, DC, 2nd edn, 1971.
29 K. Reuter and M. Scheffler, *Phys. Rev. B: Condens. Matter*, 2001, **65**, 035406.
30 K.-P. Bohnen, R. Heid and O. de la Pena Seaman, *Phys. Rev. B: Condens. Matter Mater. Phys.*, 2010, **81**, 081405.
31 J. P. Perdew, K. Burke and M. Ernzerhof, *Phys. Rev. Lett.*, 1996, **77**, 3865–3868.
32 A. Zunger, in *Statics and Dynamics of Alloy Phase Transformations*, ed. P. E. A. Turchi and A. Gonis, Springer, New York, 1994, pp. 361–419.
33 S. Piccinin and C. Stampfl, *Phys. Rev. B: Condens. Matter Mater. Phys.*, 2010, **81**, 8.
34 Y. Zhang, V. Blum and K. Reuter, *Phys. Rev. B: Condens. Matter Mater. Phys.*, 2007, **75**, 235406.
35 B. C. Han, A. Van der Ven, G. Ceder and B. J. Hwang, *Phys. Rev. B: Condens. Matter Mater. Phys.*, 2005, **72**, 205409.
36 J. T. Jankowiak and M. A. Barteau, *J. Catal.*, 2005, **236**, 366–378.
37 S. Linic, J. Jankowiak and M. A. Barteau, *J. Catal.*, 2004, **224**, 489–493.
38 F. Bocquet, C. Maurel, J.-M. Roussel, M. Abel, M. Koudia and L. Porte, *Phys. Rev. B: Condens. Matter Mater. Phys.*, 2005, **71**, 075405.
39 C. Maurel, M. Abel, M. Koudia, F. Bocquet and L. Porte, *Surf. Sci.*, 2005, **596**, 45–52.
40 S. Piccinin, C. Stampfl and M. Scheffler, *Phys. Rev. B: Condens. Matter Mater. Phys.*, 2008, **77**, 075426.
41 S. Piccinin, C. Stampfl and M. Scheffler, *Surf. Sci.*, 2009, **603**, 1467–1475.
42 S. Piccinin, S. Zafeiratos, C. Stampfl, T. W. Hansen, M. Haevecker, D. Teschner, V. I. Bukhtiyarov, F. Girgsdies, A. Knop-Gericke, R. Schloegl and M. Scheffler, *Phys. Rev. Lett.*, 2010, **104**, 035503.
43 S. Piccinin, N. L. Nguyen, C. Stampfl and M. Scheffler, *J. Mater. Chem.*, 2010, **20**, 10521–10527.
44 S. Linic and M. A. Barteau, *J. Am. Chem. Soc.*, 2003, **125**, 4034–4035.
45 M. Mavrikakis, D. J. Doren and M. A. Barteau, *J. Phys. Chem. B*, 1998, **102**, 394–399.
46 M.-L. Bocquet, A. Michaelides, D. Loffreda, P. Sautet, A. Alavi and D. A. King, *J. Am. Chem. Soc.*, 2003, **125**, 5620–5621.
47 M.-L. Bocquet and D. Loffreda, *J. Am. Chem. Soc.*, 2005, **127**, 17207–17215.
48 D. Torres, N. Lopez and F. Illas, *J. Catal.*, 2006, **243**, 404–409.
49 J. R. Kitchin, K. Reuter and M. Scheffler, *Phys. Rev. B: Condens. Matter Mater. Phys.*, 2008, **77**, 075437.
50 Y. Zhang and W. Yang, *Phys. Rev. Lett.*, 1998, **80**, 890–890.
51 B. Hammer, L. B. Hansen and J. K. Nørskov, *Phys. Rev. B: Condens. Matter*, 1999, **59**, 7413–7421.
52 E. K. Vestergaard, R. T. Vang, J. Knudsen, T. M. Pedersen, T. An, E. Laegsgaard, I. Stensgaard, B. Hammer and F. Besenbacher, *Phys. Rev. Lett.*, 2005, **95**, 126101.
53 K. J. Andersson, F. Calle-Vallejo, J. Rossmeisl and L. Chorkendorff, *J. Am. Chem. Soc.*, 2009, **131**, 2404–2407.
54 K. J. Andersson and I. Chorkendorff, *Surf. Sci.*, 2010, **604**, 1733–1736.
55 T. Ma, Q. Fu, H. Y. Su, H. Y. Liu, Y. Cui, Z. Wang, R. T. Mu, W. X. Li and X. H. Bao, *ChemPhysChem*, 2009, **10**, 1013–1016.
56 L. J. Wan, T. Moriyama, M. Ito, H. Uchida and M. Watanabe, *Chem. Commun.*, 2002, 58–59.
57 Z. Paal, A. Wootsch, D. Teschner, K. Lazar, I. E. Sajo, N. Gyorffy, G. Weinberg, A. Knop-Gericke and R. Schloegl, *Appl. Catal., A*, 2011, **391**, 377–385.
58 C. A. Menning and J. G. Chen, *J. Power Sources*, 2010, **195**, 3140–3144.
59 V. Papaefthimiou, T. Dintzer, V. Dupuis, A. Tamion, F. Tournus, D. Teschner, M. Haevecker, A. Knop-Gericke, R. Schloegl and S. Zafeiratos, *J. Phys. Chem. Lett.*, 2011, **2**, 900–904.
60 B. Bridier, J. Perez-Ramirez, A. Knop-Gericke, R. Schloegl and D. Teschner, *Chem. Sci.*, 2011, **2**, 1379–1383.
61 Z. Song, D. L. Tan, F. He and X. H. Bao, *Appl. Surf. Sci.*, 1999, **137**, 142–149.
62 Y. T. Law, T. Dintzer and S. Zafeiratos, *Appl. Surf. Sci.*, 2011, **258**, 1480–1487.
63 M. E. Grass, M. Park, F. Aksoy, Y. W. Zhang, M. Kunz, Z. Liu and B. S. Mon, *Langmuir*, 2010, **26**, 16362–16367.

64 F. Tao, M. E. Grass, Y. W. Zhang, D. R. Butcher, J. R. Renzas, Z. Liu, J. Y. Chung, B. S. Mun, M. Salmeron and G. A. Somorjai, *Science*, 2008, **322**, 932–934.
65 A. Borgna, B. G. Anderson, A. M. Saib, H. Bluhm, M. Havecker, A. Knop-Gericke, A. E. T. Kuiper, Y. Tamminga and J. W. Niemantsverdriet, *J. Phys. Chem. B*, 2004, **108**, 17905–17914.
66 K. J. J. Mayrhofer, V. Juhart, K. Hartl, M. Hanzlik and M. Arenz, *Angew. Chem., Int. Ed.*, 2009, **48**, 3529–3531.
67 R. T. Mu, Q. Fu, H. Y. Liu, D. L. Tan, R. S. Zhai and X. H. Bao, *Appl. Surf. Sci.*, 2009, **255**, 7296–7301.
68 S. M. Oxford, P. L. Lee, P. J. Chupas, K. W. Chapman, M. C. Kung and H. H. Kung, *J. Phys. Chem. C*, 2010, **114**, 17085–17091.
69 Y. Uemura, Y. Inada, K. K. Bando, T. Sasaki, N. Kamiuchi, K. Eguchi, A. Yagishita, M. Nomura, M. Tada and Y. Iwasawa, *J. Phys. Chem. C*, 2011, **115**, 5823–5833.
70 M. Dalmiglio, M. Amati, L. Gregoratti, T. O. Mentes, M. A. Nino, L. Felisari and M. Kiskinova, *J. Phys. Chem. C*, 2010, **114**, 16885–16891.
71 P. S. Dimick, J. L. Kross, E. G. Roberts, R. G. Herman, H. G. Stenger and C. E. Lyman, *Appl. Catal., B*, 2009, **89**, 1–11.
72 S. A. Tenney, W. He, C. C. Roberts, J. S. Ratliff, S. I. Shah, G. S. Shafai, V. Turkowski, T. S. Rahman and D. A. Chen, *J. Phys. Chem. C*, 2011, **115**, 11112–11123.
73 S. A. Tenney, J. S. Ratliff, C. C. Roberts, W. He, S. C. Ammal, A. Heyden and D. A. Chen, *J. Phys. Chem. C*, 2010, **114**, 21652–21663.
74 M. Garcia-Mota and N. Lopez, *Phys. Rev. B: Condens. Matter Mater. Phys.*, 2010, **82**, 9.
75 K. Sasaki, K. A. Kuttiyiel, L. Barrio, D. Su, A. I. Frenkel, N. Marinkovic, D. Mahajan and R. R. Adzic, *J. Phys. Chem. C*, 2011, **115**, 9894–9902.
76 N. Y. Topsoe and H. Topsoe, *J. Mol. Catal. A: Chem.*, 1999, **141**, 95–105.
77 J. D. Grunwaldt, A. M. Molenbroek, N. Y. Topsoe, H. Topsoe and B. S. Clausen, *J. Catal.*, 2000, **194**, 452–460.
78 J. R. Renzas, W. Y. Huang, Y. W. Zhang, M. E. Grass, D. T. Hoang, S. Alayoglu, D. R. Butcher, F. Tao, Z. Liu and G. A. Somorjai, *Phys. Chem. Chem. Phys.*, 2011, **13**, 2556–2562.
79 J. R. Renzas, W. Y. Huang, Y. W. Zhang, M. E. Grass and G. A. Somorjai, *Catal. Lett.*, 2011, **141**, 235–241.
80 F. Gao, Y. L. Wang and D. W. Goodman, *J. Phys. Chem. C*, 2009, **113**, 14993–15000.
81 F. Gao, Y. L. Wang and D. W. Goodman, *J. Catal.*, 2009, **268**, 115–121.
82 F. Gao, Y. L. Wang and D. W. Goodman, *J. Am. Chem. Soc.*, 2009, **131**, 5734–5735.
83 F. Gao, Y. L. Wang and D. W. Goodman, *J. Phys. Chem. C*, 2010, **114**, 4036–4043.
84 M. Garcia-Mota and N. Lopez, *Phys. Rev. B: Condens. Matter Mater. Phys.*, 2010, **82**, 075411.
85 V. Soto-Verdugo and H. Metiu, *Surf. Sci.*, 2007, **601**, 5332–5339.
86 H. Guesmi, C. Louis and L. Delannoy, *Chem. Phys. Lett.*, 2011, **503**, 97–100.
87 S. Alayoglu, F. Tao, V. Altoe, C. Specht, Z. W. Zhu, F. Aksoy, D. R. Butcher, R. J. Renzas, Z. Liu and G. A. Somorjai, *Catal. Lett.*, 2011, **141**, 633–640.
88 X. Y. Liu, A. Q. Wang, L. Li, T. Zhang, C. Y. Mou and J. F. Lee, *J. Catal.*, 2011, **278**, 288–296.
89 J. L. Margitfalvi, I. Borbath, K. Lazar, E. Tfirst, A. Szegedi, M. Hegedus and S. Gobolos, *J. Catal.*, 2001, **203**, 94–103.
90 H. Y. Su, X. K. Gu, X. F. Ma, Y. H. Zhao, X. H. Bao and W. X. Li, *Catal. Today*, 2011, **165**, 89–95.
91 M. Garcia-Mota and N. Lopez, *Phys. Chem. Chem. Phys.*, 2011, **13**, 5790–5797.
92 J. A. Anderson, M. Fernandez-Garcia and G. L. Haller, *J. Catal.*, 1996, **164**, 477–483.
93 N. Iwasa, S. Masuda, N. Ogawa and N. Takezawa, *Appl. Catal., A*, 1995, **125**, 145–157.
94 K. Fottinger, J. A. van Bokhoven, M. Nachtegaal and G. Rupprechter, *J. Phys. Chem. Lett.*, 2011, **2**, 428–433.
95 C. Rameshan, W. Stadlmayr, C. Weilach, S. Penner, H. Lorenz, M. Hävecker, R. Blume, T. Rocha, D. Teschner, A. Knop-Gericke, R. Schlögl, N. Memmel, D. Zemlyanov, G. Rupprechter and B. Klötzer, *Angew. Chem., Int. Ed.*, 2010, **49**, 3224–3227.
96 C. Rameshan, C. Weilach, W. Stadlmayr, S. Penner, H. Lorenz, M. Havecker, R. Blume, T. Rocha, D. Teschner, A. Knop-Gericke, R. Schlogl, D. Zemlyanov, N. Memmel, G. Rupprechter and B. Klotzer, *J. Catal.*, 2010, **276**, 101–113.
97 S. Zafeiratos, F. Paloukis, G. Papakonstantinou, D. Teschner, M. Havecker, E. Vass, P. Schnorch, A. Knop-Gericke, R. Schlogl, B. Moreno, E. Chinarro, J. R. Jurado and S. G. Neophytides, *Catal. Today*, 2010, **157**, 250–256.
98 J. Shu, B. E. W. Bongondo, B. P. A. Grandjean, A. Adnot and S. Kaliaguine, *Surf. Sci.*, 1993, **291**, 129–138.
99 S. Gonzalez, K. M. Neyman, S. Shaikhutdinov, H. J. Freund and F. Illas, *J. Phys. Chem. C*, 2007, **111**, 6852–6856.
100 D. Teschner, J. Borsodi, A. Wootsch, Z. Revay, M. Haevecker, A. Knop-Gericke, S. D. Jackson and R. Schloegl, *Science*, 2008, **320**, 86–89.
101 D. Teschner, Z. Revay, J. Borsodi, M. Haevecker, A. Knop-Gericke, R. Schloegl, D. Milroy, S. D. Jackson, D. Torres and P. Sautet, *Angew. Chem., Int. Ed.*, 2008, **47**, 9274–9278.
102 D. Teschner, J. Borsodi, Z. Kis, L. Szentmiklosi, Z. Revay, A. Knop-Gericke, R. Schloegl, D. Torres and P. Sautet, *J. Phys. Chem. C*, 2010, **114**, 2293–2299.
103 M. Garcia-Mota, B. Bridier, J. Perez-Ramirez and N. Lopez, *J. Catal.*, 2010, **273**, 92–102.
104 P. Tiruppathi, J. J. Low, A. S. Y. Chan, S. R. Bare and R. J. Meyer, *Catal. Today*, 2011, **165**, 106–111.
105 Y. M. Jin, A. K. Datye, E. Rightor, R. Gulotty, W. Waterman, M. Smith, M. Holbrook, J. Maj and J. Blackson, *J. Catal.*, 2001, **203**, 292–306.
106 L. Piccolo, A. Piednoir and J. C. Bertolini, *Surf. Sci.*, 2005, **592**, 169–181.
107 A. Hugon, L. Delannoy, J. M. Krafft and C. Louis, *J. Phys. Chem. C*, 2010, **114**, 10823–10835.
108 M. Di Vece, S. Bals, J. Verbeeck, P. Lievens and G. Van Tendeloo, *Phys. Rev. B: Condens. Matter Mater. Phys.*, 2009, **80**, 125420.
109 N. Lopez and C. Vargas-Fuentes, *Chem. Commun.*, 2012, **48**, 1379–1391.
110 T. C. Q. Noakes, P. Bailey, S. Laroze, L. H. Bloxham, R. Raval and C. J. Baddeley, *Surf. Interface Anal.*, 2000, **30**, 81–84.
111 A. G. Trant, T. E. Jones, T. C. Q. Noakes, P. Bailey and C. J. Baddeley, *Surf. Sci.*, 2010, **604**, 300–307.
112 T. E. Jones, T. C. Q. Noakes, P. Bailey and C. J. Baddeley, *Surf. Sci.*, 2004, **569**, 63–75.
113 R. Hirschl, F. Delbecq, P. Sautet and J. Hafner, *J. Catal.*, 2003, **217**, 354–366.
114 F. Studt, F. Abild-Pedersen, T. Bligaard, R. Z. Sorensen, C. H. Christensen and J. K. Norskov, *Science*, 2008, **320**, 1320–1322.
115 B. Bridier and J. Perez-Ramirez, *J. Am. Chem. Soc.*, 2010, **132**, 4321–4327.
116 D. Ferri, M. S. Kumar, R. Wirz, A. Eyssler, O. Korsak, P. Hug, A. Weidenkaff and M. A. Newton, *Phys. Chem. Chem. Phys.*, 2010, **12**, 5634–5646.
117 J. K. Norskov, T. Bligaard, J. Rossmeisl and C. H. Christensen, *Nat. Chem.*, 2009, **1**, 37–46.
118 K. Reuter, in *Modelling Heterogeneous Catalytic Reactions: From the Molecular Process to the Technical System*, ed. O. Deutschmann, Wiley-VCH, Weinheim, 2011.
119 K. Reuter and M. Scheffler, *Phys. Rev. B: Condens. Matter Mater. Phys.*, 2006, **73**, 045433.
120 J. Rogal, K. Reuter and M. Scheffler, *Phys. Rev. B: Condens. Matter Mater. Phys.*, 2008, **77**, 155410.